An approximation of the M 2 closure: application to radiotherapy dose simulation

T Pichard, G W Alldredge, Stéphane Brull, B Dubroca, M Frank

Noname manuscript No.
(will be inserted by the editor)

An approximation of the M_2 closure: application to radiotherapy dose simulation

T. Pichard · G.W. Alldredge · S. Brull · B. Dubroca · M. Frank

the date of receipt and acceptance should be inserted later

Abstract Particle transport in radiation therapy can be modelled by a kinetic equation which must be solved numerically. Unfortunately, the numerical solution of such equations is generally too expensive for applications in medical centers. Moment methods provide a hierarchy of models used to reduce the numerical cost of these simulations while preserving basic properties of the solutions. Moment models require a closure because they have more unknowns than equations. The entropy-based closure is based on the physical description of the particle interactions and provides desirable properties. However, computing this closure is expensive. We propose an approximation of the closure for the first two models in the hierarchy, the M_1 and M_2 models valid in one, two or three dimensions of space. Compared to other approximate closures, our method works in multiple dimensions. We obtain the approximation by a careful study of the domain of realizability and by invariance properties of the entropy minimizer. The M_2 model is shown to provide significantly better accuracy than the M_1 model for the numerical simulation of a dose computation in radiotherapy. We propose a numerical solver using those approximated closures. Numerical experiments in dose computation test cases show that the new method is more efficient compared to numerical solution of the minimum entropy problem using standard software tools.

Keywords Moment models, Entropy-based closure, Radiotherapy dose computation

Mathematics Subject Classification (2000) 82C70, 82D99, 94A17

1 Introduction

The aim of radiation treatments is to destroy tumor cells by prescribing a certain quantity of energy, called the dose, to the tumor cells. This dose is produced by radiation which can be

T. Pichard · B. Dubroca
CELIA, Université de Bordeaux, 351 cours de la libération, 33400 Talence, France, pichard@mathcces.rwth-aachen.de, +335 40 00 37 62 ·
T. Pichard · G.W. Alldredge · M. Frank
MathCCES, RWTH Aachen University, Schinkelstr. 2., 52062, Aachen, Germany ·
S. Brull
IMB, Université de Bordeaux, 351 cours de la libération, 33400 Talence, France

modelled by the transport of particles (photons, electrons, protons, hadrons, depending on the type of radiation).

A large range of numerical approaches has been proposed in the literature to compute the dose. Dose distributions are typically numerically computed using Monte-Carlo algorithms (see e.g. [20]) or discrete-ordinate methods (see e.g. [35]). However such direct solution methods often require more computing resources than are typically available in medical centers. Resource effective alternatives to those approaches (see e.g. [39] and references therein), used in medical centers, include semi-empirical methods (e.g. Fermi-Eyges methods), probabilistic methods (fast Monte Carlo simulations, see e.g. [52,14,55] and references therein) and PDE-based methods ([54]). However those alternatives may be unprecise for certain applications. The present method is an in-between alternative with an accuracy comparable to Monte-Carlo and much lower computational costs.

This paper is a follow-up to [19,46,12]. The aim is to propose a PDE-based numerical approach which is fast and accurate enough for practical applications. We study in the next section a moment approach, i.e. a PDE-based approach, which has a much lower numerical cost than the Monte-Carlo methods.

The transport of particles for radiotherapy problem can be described by kinetic models ([29,44]) for the fluence ψ of the particles. Due to the high dimensionality of the fluence (it depends on position $x \in \mathbb{R}^3$, energy $\varepsilon \in \mathbb{R}^+$ and direction of flight $\Omega \in S^2$ where S^2 is the unit sphere), solving the kinetic transport equations is numerically expensive. The kinetic model can be reduced by extracting angular moments. The resulting models retain the major properties of the kinetic models.

Those models were applied in a large range of physics, such as fluid dynamics ([22,34, 41]), plasma physics ([23,24,36,37]), semi-conductors ([4,49]) or radiative transfer ([13, 17,33,6,11]).

The main difficulty arising when deriving moment models is computing a closure. Indeed moments equations have more unknowns than equations, therefore a closure needs to be computed. This closure is generally chosen to retrieve the basic features of the underlying kinetic models. Generally, one constructs an ansatz ψ_R for the exact fluence so that the ansatz satisfies certain integral constraints. The closure is then computed by replacing the exact fluence with the ansatz.

In the present paper, an entropy-based closure is chosen which leads to the hierarchy of moment models colloquially known as M_N, where N indicates the highest order of the moments in the model. This closure is based on the physics of the collisions and leads to a hyperbolic system of moment equations with an entropy dissipation property ([34]). However, computing such a closure directly requires solving (numerically) a minimization problem at every point in space and energy. Furthermore, the solution of this minimization problem requires repeated expensive quadrature computations ([27,2,1]). The main goal of this paper is to provide an approximation of the M_1 and the M_2 closures which avoids the optimization problem and the quadrature computations therein. We obtain the approximation by a careful study of the domain of realizability and by invariance properties of the entropy minimizer. There exist many approximate moment closures, e.g. the main alternative being the P_N closures. However, they present drawbacks conflicting with the applications we have in mind. Especially, several of them are only derived in one space dimension (see e.g. [50, 53,3]), and it is not entirely clear how to generalize the ideas to multiple dimensions. In this paper we deal with the case of multiple dimensions.

In the next section, a simplified kinetic model of the transport of electrons is described, the procedure of moment extraction is presented and illustrated through the M_1 model and the advantages of the M_2 model are shown. The main result is presented in Section 3, it

consists of an approximation of the M_2 closure for three dimensional problems. In order to validate our approach, the kinetic and moment models are compared on numerical test cases from medical applications in Section 4. The last section is devoted to conclusions and perspectives.

2 Models

The transport of electrons in the field of radiotherapy can be modeled using kinetic theory. We first recall a kinetic model used in the field of medical physics ([29,19]), then the procedure of moment extraction, which is afterward illustrated through the first model in the hierarchy of entropy based moment models, the M_1 model.

2.1 Kinetic model

In this study, only the transport of electrons is considered. The transport of photons with the approach described in this paper has been studied in [45]. We consider here only Møller's and Mott's collisions for electrons (see [29] and references therein). Mott's collisions are elastic. Møller's collisions are inelastic and are ionizing interactions, i.e. two electrons emerge from this collision, a primary (the more energetic one) and a secondary. The electron transport can be modelled by the following kinetic equation [29,19]

$$\Omega.\nabla_x \psi(x,\Omega,\varepsilon) = \rho(x) Q(\psi)(x,\Omega,\varepsilon). \tag{1}$$

The unknown ψ is the fluence of electrons depending on position $x \in Z$, energy $\varepsilon \in [0,\varepsilon_{max}]$, direction of flight $\Omega \in S^2$, and Q is the collision operator. For Mott's and Møller's collisions, the collision can be represented by linear Boltzmann (LB) gain and loss terms

$$\begin{aligned} Q(\psi)(x,\Omega,\varepsilon) = &\int_{S^2}\int_{\varepsilon}^{\infty} (\sigma_{M,1}+\sigma_{M,2})(\varepsilon',\varepsilon,\Omega'.\Omega)\psi(x,\Omega',\varepsilon')d\varepsilon' d\Omega' - \sigma_{T,M}(\varepsilon)\psi(x,\Omega,\varepsilon) \\ &+ \int_{S^2} \sigma_{Mott}(\varepsilon,\Omega'.\Omega)\psi(x,\Omega',\varepsilon)d\Omega' - \sigma_{T,Mott}(\varepsilon)\psi(x,\Omega,\varepsilon). \end{aligned} \tag{2}$$

The gain terms are characterized by the differential cross sections for Mott's and Møller's primary and secondary electrons σ_{Mott}, $\sigma_{M,1}$, $\sigma_{M,2}$, and the loss terms by the total cross sections $\sigma_{M,T}$ and $\sigma_{T,Mott}$. The superscript $'$ refers to the state of the particle before collision; the absence of this superscript refers to the post-collisional state. $\rho(x)$ is the density of atomic cores in the medium at position x. Møller's cross section for primary electrons $\sigma_{M,1}$ is very peaked in energy, meaning that most of the particles lose small energy during those collisions. Due to that peak in the cross section, the continuous-slowing down approximation (CSD, see [48,44]) can be applied here, and the deflection due to Møller's effect is negligible compared to the one due to Mott's effect. This leads to approximating ([32,19,44])

$$\begin{aligned} Q(\psi)(x,\Omega,\varepsilon) \approx Q_{CSD}(\psi)(x,\Omega,\varepsilon) &= \partial_\varepsilon(S\psi)(x,\Omega,\varepsilon) \\ &+ \int_{S^2}\int_{\varepsilon}^{\infty} \sigma_{M,2}(\varepsilon',\varepsilon,\Omega'.\Omega)\psi(x,\Omega',\varepsilon')d\varepsilon' d\Omega' \\ &+ \int_{S^2} \sigma_{Mott}(\varepsilon,\Omega'.\Omega)\psi(x,\Omega',\varepsilon)d\Omega' - \sigma_{T,Mott}(\varepsilon)\psi(x,\Omega,\varepsilon), \end{aligned} \tag{3}$$

where the stopping power S characterizes this energy loss.

Similarily, the remaining elastic cross section σ_{Mott} is forward-peaked, meaning that most of the particles are slightly deflected during those collisions. Due to that peak in the cross section, the collision operator can be approximated by a Fokker-Planck (FP, see [48] although the validity of this approximation was discussed in [44]) operator

$$\begin{aligned} Q_{CSD}(\psi)(x,\Omega,\varepsilon) \approx Q_{FP}(\psi)(x,\Omega,\varepsilon) &= \partial_\varepsilon(S\psi)(x,\Omega,\varepsilon) \\ &+T(\varepsilon)\left[\partial_\mu\left((1-\mu^2)\partial_\mu\psi\right)(x,\Omega,\varepsilon)+\frac{1}{1-\mu^2}\partial_\phi^2\psi(x,\Omega,\varepsilon)\right] \\ &+\int_{S^2}\int_\varepsilon^\infty \sigma_{M,2}(\varepsilon',\varepsilon,\Omega'.\Omega)\psi(x,\Omega',\varepsilon')d\varepsilon' d\Omega', \end{aligned} \tag{4}$$

where the transport coefficient $T(\varepsilon)$ characterizes this deflection, μ and ϕ are such that $\Omega = (\mu, \sqrt{1-\mu^2}\cos\phi, \sqrt{1-\mu^2}\sin\phi)$.

2.2 Moment models

A moment model is a reduction of a kinetic model that requires much lower computational times (see e.g. comparisons in Section 4). One can reduce the number of variables by approximating the angular distribution by an ansatz $\psi \approx \psi_R(\Omega)$ satisfying integral constraints.

Let us define ψ^i as the moment of order i of ψ, namely

$$\psi^i := \left\langle \underbrace{\Omega\otimes\cdots\otimes\Omega}_{\text{i times}}\psi \right\rangle = \int_{S^2}\Omega\otimes\cdots\otimes\Omega\,\psi d\Omega.$$

Here $\otimes$ denotes the tensor product. Instead of working with ψ which depends on ε, x and Ω, the moments ψ^i of order 0 to N are studied.

One obtains equations for the moments ψ^i by extracting moments of (1)

$$\nabla_x.\psi^{i+1}(x,\varepsilon) = \rho(x)Q^i(\psi^i)(x,\varepsilon), \tag{5}$$

where the moments of order 0 to 2 of the collision operator read

$$Q^0(\psi^0)(x,\varepsilon) = \int_\varepsilon^\infty \sigma_M^0(\varepsilon',\varepsilon)\psi^0(x,\varepsilon')d\varepsilon' - (\sigma_{T,M}+\sigma_{T,Mott}-\sigma_{Mott}^0)(\varepsilon), \tag{6a}$$

$$Q^1(\psi^1)(x,\varepsilon) = \int_\varepsilon^\infty \sigma_M^1(\varepsilon',\varepsilon)\psi^1(x,\varepsilon')d\varepsilon' - (\sigma_{T,M}+\sigma_{T,Mott}-\sigma_{Mott}^1)(\varepsilon)\psi^1(x,\varepsilon') \tag{6b}$$

$$\begin{aligned} Q^2(\psi^2)(x,\varepsilon) = &\int_\varepsilon^\infty \frac{\sigma_M^0-\sigma_M^2}{2}(\varepsilon',\varepsilon)tr(\psi^2)(x,\varepsilon')Id + \frac{3\sigma_M^2-\sigma_M^0}{2}(\varepsilon',\varepsilon)\psi^2(x,\varepsilon')d\varepsilon' \\ &+\frac{\sigma_{Mott}^0-\sigma_{Mott}^2}{2}(\varepsilon)tr(\psi^2)(x,\varepsilon)Id + \frac{3\sigma_{Mott}^2-\sigma_{Mott}^0}{2}(\varepsilon)\psi^2(x,\varepsilon) \\ &-(\sigma_{T,M}+\sigma_{T,Mott})(\varepsilon)\psi^1(x,\varepsilon') \end{aligned} \tag{6c}$$

where $\sigma_M = \sigma_{M,1}+\sigma_{M,2}$ and σ^i are scalars given by

$$\sigma^i(\varepsilon',\varepsilon) = 2\pi\int_{-1}^{+1}\mu^i\sigma(\varepsilon',\varepsilon,\mu)d\mu.$$

Similarily the moments of the CSD operator (3) and the FP operator (4) yield

$$\begin{aligned} Q^0_{CSD}(\psi^0)(x,\varepsilon) =& \partial_\varepsilon(S\psi^0)(x,\varepsilon) \\ &+ \int_\varepsilon^\infty \sigma^0_{M,2}(\varepsilon',\varepsilon)\psi^0(x,\varepsilon')d\varepsilon' - (\sigma_{T,Mott} - \sigma^0_{Mott})(\varepsilon)\psi^0(x,\varepsilon), \end{aligned} \tag{7a}$$

$$\begin{aligned} Q^1_{CSD}(\psi^1)(x,\varepsilon) =& \partial_\varepsilon(S\psi^1)(x,\varepsilon) \\ &+ \int_\varepsilon^\infty \sigma^1_{M,2}(\varepsilon',\varepsilon)\psi^1(x,\varepsilon')d\varepsilon' - (\sigma_{T,Mott} - \sigma^1_{Mott})(\varepsilon)\psi^1(x,\varepsilon), \end{aligned} \tag{7b}$$

$$\begin{aligned} Q^2_{CSD}(\psi^2)(x,\varepsilon) =& \partial_\varepsilon(S\psi^2)(x,\varepsilon) \\ &+ \int_\varepsilon^\infty \frac{\sigma^0_{M,2} - \sigma^2_{M,2}}{2}(\varepsilon',\varepsilon)tr(\psi^2)(x,\varepsilon')Id + \frac{3\sigma^2_{M,2} - \sigma^0_{M,2}}{2}(\varepsilon',\varepsilon)\psi^2(x,\varepsilon')d\varepsilon' \\ &+ \frac{\sigma^0_{Mott} - \sigma^2_{Mott}}{2}(\varepsilon)tr(\psi^2)(x,\varepsilon)Id + \frac{3\sigma^2_{Mott} - \sigma^0_{Mott}}{2}(\varepsilon)\psi^2(x,\varepsilon) \\ &- \sigma_{T,Mott}(\varepsilon)\psi^2(x,\varepsilon), \end{aligned} \tag{7c}$$

$$Q^0_{FP}(\psi^0)(x,\varepsilon) = \partial_\varepsilon(S\psi^0)(x,\varepsilon) + \int_\varepsilon^\infty \sigma^0_{M,2}(\varepsilon',\varepsilon)\psi^0(x,\varepsilon')d\varepsilon', \tag{8a}$$

$$Q^1_{FP}(\psi^1)(x,\varepsilon) = \partial_\varepsilon(S\psi^1)(x,\varepsilon) - 2T(\varepsilon)\psi^1(x,\varepsilon) + \int_\varepsilon^\infty \sigma^1_{M,2}(\varepsilon',\varepsilon)\psi^1(x,\varepsilon')d\varepsilon', \tag{8b}$$

$$\begin{aligned} Q^2_{FP}(\psi^2)(x,\varepsilon) =& \partial_\varepsilon(S\psi^2)(x,\varepsilon) - 2T(\varepsilon)\left(3\psi^2(x,\varepsilon) - tr(\psi^2)(x,\varepsilon)Id\right) \\ &+ \int_\varepsilon^\infty \frac{\sigma^0_{M,2} - \sigma^2_{M,2}}{2}(\varepsilon',\varepsilon)tr(\psi^2)(x,\varepsilon')Id + \frac{3\sigma^2_{M,2} - \sigma^0_{M,2}}{2}(\varepsilon',\varepsilon)\psi^2(x,\varepsilon')d\varepsilon'. \end{aligned} \tag{8c}$$

Remark that the only difference between the moments of the CSD and FP operators are the scalars before $\psi^2(x,\varepsilon)$ and $tr(\psi^2)(x,\varepsilon)Id$.

The system (5) requires a closure, as it has more unknown than equations. In practice, this is done by approximating ψ by an ansatz ψ_R, and then computing the higher-order term using this ansatz, i.e.

$$\psi^{N+1} \approx \left\langle \underbrace{\Omega \otimes \cdots \otimes \Omega}_{\text{N+1 times}} \psi_R \right\rangle,$$

where ψ_R is an ansatz having the moments $(\psi^0, ..., \psi^N)$.

For $N = 2$, choosing an ansatz ψ_R provides an approximation of the flux ψ^3 depending on (ψ^0, ψ^1, ψ^2). For each possible set of moments (ψ^0, ψ^1, ψ^2), one needs to find an ansatz ψ_R having the right moments. This problem can be written as

$$\text{find} \quad \psi_R(\Omega), \quad \text{s.t.} \quad \left\langle \underbrace{\Omega \otimes \cdots \otimes \Omega}_{\text{i times}} \psi_R \right\rangle = \psi^i, \quad i = 0, ..., 2.$$

One possibility is simply to choose the ansatz ψ_R as a polynomial of degree N

$$\psi_R(\Omega) = \bar{\lambda}.\bar{m}(\Omega).$$

Here $\bar{m}(\Omega)$ is a basis of polynomial of degree N over S^2, in particular, we chose

$$\text{for} \quad N = 1, \quad \bar{m}(\Omega) = (1, \quad \Omega_1, \quad \Omega_2, \quad \Omega_3),$$
$$\text{for} \quad N = 2, \quad \bar{m}(\Omega) = \left(\Omega_1, \quad \Omega_2, \quad \Omega_3, \quad \Omega_1^2, \quad \Omega_2^2, \quad \Omega_3^2, \quad \Omega_1\Omega_2, \quad \Omega_1\Omega_3, \quad \Omega_2\Omega_3\right)$$

in the rest of the paper and $\bar{\lambda}$ is the unique vector of scalars such that the moments of ψ_R are $(\psi^0,...,\psi^N)$. This leads to the so-called P_N models. Computing the ansatz (and then the closure) is simple and only requires the solution of a linear systems. However, P_N models present several drawbacks. First the obtained function ψ_R can be negative (see e.g. [26,40]), which is not physical. Second, in radiotherapy beams of particles are used. Perfect beams can be modeled by Dirac distribution in Ω. Such distributions are poorly approximated by polynomials.

Example 1 Consider a Dirac peak $\psi = \delta(\Omega.e_1 - 1)$. Its first moments read

$$\psi^0 = \langle \psi \rangle = 1, \qquad \psi^1 = \langle \Omega \psi \rangle = e_1.$$

The polynomial $\psi_R \in \mathbb{R}^1[X]$ of degree 1 having ψ^0 and ψ^1 for moments reads

$$\psi_R(\Omega) = \frac{1+3\Omega_1}{2}.$$

One first remark that the P_1 ansatz differs from the beam distribution. Then computing the second order moment of this ansatz, i.e. the P_1 closure, read

$$\langle \Omega \otimes \Omega \psi_R(\Omega) \rangle = Diag\left(\frac{1}{3}, \frac{1}{3}, \frac{1}{3}\right) \neq e_1 \otimes e_1 = \langle \Omega \otimes \Omega \psi \rangle,$$

which differs from the second order moment of the Dirac peak, and therefore the P_1 model is not able to represent a beam. Similar computations show that for any N the P_N model is also not able to capture the exact closure. One solution to obtain a good accuracy with the P_N model when considering beams of particles consists in chosing the number of moments N large, which deteriorates the time efficiency of the method.

Among the possible candidates for ψ_R (having the moments $(\psi^0,...,\psi^N)$), we chose the one that minimizes Boltzmann entropy function

$$\mathscr{H}(f) = \int_{S^2} (f\log(f) - f)(\Omega) d\Omega, \tag{9}$$

which leads to the hierarchy of the so-called M_N models.

Theorem 1 ([42,8,9,10,30,51,28]) *Consider a vector of polynomials $\bar{m}(\Omega)$ and a vector $\bar{\psi}$ such that there exists at least one positive function $\psi > 0$ satisfying*

$$\bar{\psi} = \langle \bar{m} \psi \rangle.$$

Then there exists a unique minimizer ψ_R to (9) *which has the form*

$$\psi_R(\Omega) = \exp(\bar{\lambda}.\bar{m}(\Omega)). \tag{10}$$

Furthermore, the function that sends the moments $\bar{\psi}$ onto the ansatz (10) *is a smooth bijection.*

Beam-like distributions can be correctly approximated by ansätze of the form (10). Indeed, a perfect beam in the direction Ω_0 can be modeled by the Dirac distribution, which can be interpreted as the limit of a sequence of M_1 ansätze

$$\delta(\Omega.\Omega_0 - 1) = \lim_{n\to+\infty} \frac{1}{2\pi} \exp\left((\log(n) - n) + n\Omega.\Omega_0\right).$$

In this sense beam-like distributions are in the closure of the set of distributions of the form (10).

In the next section, we focus on the following two properties of the M_N model (and especially of the M_2 model) when constructing the approximation of the M_2 closure.

Hyperbolicity The M_N equations are known to be symmetric hyperbolic ([34,21]). This means that the Jacobian of the flux

$$J = \nabla_{(\psi^0,...,\psi^N)}(\psi^1,...,\psi^{N+1})$$

is diagonalizable with real eigenvalues.

Realizability The solution ψ to the kinetic equation 1, with the collision operator (2), (3) or (4), is positive. The realizability property corresponds to requiring that the solution $(\psi^0,...,\psi^N)$ to the moments system (5) with the associated collision operator (6), (7) or (8) are the moments of one positive distribution ψ, i.e.

$$\exists \psi(\Omega) > 0, \quad \text{s.t.} \quad (\psi^0,...,\psi^N) = \int_{S^2} (1,...,\underbrace{\Omega \otimes \cdots \otimes \Omega}_{\text{N times}}) \psi(\Omega) d\Omega.$$

Definition 1 The set of all realizable moments of order up to N is called the realizability domain $\mathscr{R}_N$ of order N

$$\mathscr{R}_N = \left\{ \int_{S^2} (1,...,\underbrace{\Omega \otimes \cdots \otimes \Omega}_{\text{N times}}) \psi(\Omega) d\Omega, \quad \forall \psi > 0 \right\}. \tag{11}$$

Remark 1 The notion of realizability can be extended to general measures. In this paper, we avoid the technicalities associated to measures and always write non-negative densities, which formally includes the case of a sum of Diracs to represent a discrete measure.

Remark 2 The realizability domain is a convex cone. This means that positive combinations of two realizable moments is realizable. Indeed suppose $\alpha_1 > 0$ and $\alpha_2 > 0$ are two positive scalars and ψ_1 and ψ_2 are two positive functions of Ω and

$$\bar{\psi}_1 = \left\langle (1,...,\underbrace{\Omega \otimes \cdots \otimes \Omega}_{\text{N times}}) \psi_1 \right\rangle, \quad \bar{\psi}_2 = \left\langle (1,...,\underbrace{\Omega \otimes \cdots \otimes \Omega}_{\text{N times}}) \psi_2 \right\rangle.$$

Then the sum

$$\alpha_1 \bar{\psi}_1 + \alpha_2 \bar{\psi}_2 = \left\langle (1,...,\underbrace{\Omega \otimes \cdots \otimes \Omega}_{\text{N times}}) (\alpha_1 \psi_1 + \alpha_2 \psi_2) \right\rangle$$

is obviously realizable since $\alpha_1 \psi_1 + \alpha_2 \psi_2$ is positive. This property will be used below in Subsection 3.3 to enforce realizability of the approximated closure.

The coefficients of $\bar{\lambda}$ are generally determined by solving the dual minimization problem ([27,2,1])

$$\bar{\lambda} = \underset{\bar{a}}{\operatorname{argmin}} \langle \exp(\bar{a}.\bar{m}(\Omega)) \rangle - \bar{a}.\bar{\psi}, \tag{12}$$

where $\bar{\psi} = \langle \bar{m}(\Omega)\psi \rangle$ are the moments ψ^i associated to $\bar{m}(\Omega)$ arranged as a column vector.

Solving this minimization problem is however computationally expensive (see e.g. comparison in Section 4). Therefore we propose an alternative for the first two models in the hierarchy, the M_1 and M_2 models. It consists in smooth approximations preserving several important properties of the exact closure.

2.3 The M_1 model

We illustrate here the procedure described above for the first model in the hierarchy and propose an approximation of the closure. Considering only equations (5) for $i = 1,2$, we need to express ψ^2 as a function of ψ^0 and ψ^1. In that case, using (10), ψ_R yields

$$\psi_R(\Omega) = \exp(\lambda_0 + \lambda_1\Omega_1 + \lambda_2\Omega_2 + \lambda_3\Omega_3). \tag{13}$$

Then the coefficients $\lambda_0 \in \mathbb{R}$ and $(\lambda_1,\lambda_2,\lambda_3) \in \mathbb{R}^3$ are such that ψ_R has the right moments

$$\langle \psi_R(\Omega)\rangle = \psi^0, \quad \langle \Omega\,\psi_R(\Omega)\rangle = \psi^1.$$

Let us write $n = \psi^1/|\psi^1|$. Using rotational invariance ([33]), one can prove that there exists $\alpha \in \mathbb{R}$ such that $(\lambda_1,\lambda_2,\lambda_3) = \alpha n$.

Using this form of the ansatz ψ_R leads to

$$\frac{||\psi^1||_2}{\psi^0} = \frac{|\alpha| coth(|\alpha|) - 1}{|\alpha|} = f(|\alpha|). \tag{14}$$

This function f is bijection between $\mathbb{R}^+$ and $[0,1[$. Computing the closure ψ^2 leads to

$$\psi^2 = \psi^0\left(\frac{1-\chi_2}{2}Id + \frac{3\chi_2-1}{2}n\otimes n\right), \tag{15}$$

$$\chi_2\left(\frac{||\psi^1||_2}{\psi^0}\right) = \frac{\int_{-1}^{+1}\mu^2\exp(\alpha\mu)d\mu}{\int_{-1}^{+1}\exp(\alpha\mu)d\mu} = 1 + \frac{2}{|\alpha|}\left(1 + coth\left(|\alpha|\right)\right),$$

where $|\alpha|$ is a function of $\frac{||\psi^1||_2}{\psi^0}$ given by (14), i.e.

$$|\alpha| = f^{-1}\left(\frac{||\psi^1||_2}{\psi^0}\right).$$

The Eddington factor χ_2 does not have an analytical formula but can be approximated (see below in Section 3.3).

The M_1 model is often used because it is simple to implement and covers a large range of physical phenomena. However it presents also several drawbacks. These drawbacks are presented in the next section in order to highlight the advantages of the M_2 model compared to the M_1 model. Then an approximation of the M_2 closure is proposed. Section 4 illustrates the efficiency of the M_2 model through numerical test cases.

2.4 The advantages of the M_2 model

Now we motivate the advance to the M_2 model, that is, increasing the moment order to two. The M_2 model is able to model a larger range of physical phenomena than the M_1 model.

First, the physics are modeled more accurately. Indeed decomposing the differential cross sections into polynomials reads

$$\sigma(\varepsilon',\varepsilon,\mu) = \sum_{i=0}^{\infty}\sigma^i(\varepsilon',\varepsilon)\mu^i.$$

Then extracting the N first moments of the collisional operator is equivalent to truncating this expansion at degree N. So clearly the collisions are better modelled as N increases. This phenomenon is illustrated through the test cases in Sections 4.2 and 4.4 below.

Furthermore, M_1 is not able to distinguish certain multiple-beam cases which are of major importance in the field of radiotherapy. Indeed in external radiotherapy, the source of particles creating the dose are beams of particles applied on the boundary of a medium (see e.g. the numerical test cases in Section 4).

Example 2 Let us consider two perfect beams of opposite direction $\pm e_1$ crossing each other. This is modelled by a distribution composed of two Dirac peaks

$$\psi = \delta(\Omega.e_1 - 1) + \delta(\Omega.(-e_1) - 1).$$

Extracting the moments of this distribution yields

$$\begin{aligned}
\psi^0 &= \quad \langle \psi \rangle \quad &&= 2, \\
\psi^1 &= \quad \langle \Omega \psi \rangle \quad &&= 0_{\mathbb{R}^3}, \\
\psi^2 &= \langle \Omega \otimes \Omega \psi \rangle &&= 2 e_1 \otimes e_1.
\end{aligned}$$

Working with the M_1 model means working with (ψ^0, ψ^1). In that case, the first two moments are the same of those of an isotropic distribution $\psi = \frac{1}{2\pi}$. This means that the M_1 model is unable to distinguish two beams from a isotropic distribution. This produces an overestimation of the diffusion at the point where the beams cross each other. However with ψ^2 available, the M_2 model is able to recognize that the underlying distribution is not isotropic.

This problem also appears more generally for two-beam distributions.

Example 3 A distribution of two beams in directions e_1 and e_2

$$\psi = \delta(\Omega.e_1 - 1) + \delta(\Omega.e_2 - 1)$$

has moments

$$\begin{aligned}
\psi^0 &= \quad \langle \psi \rangle \quad &&= 2, \\
\psi^1 &= \quad \langle \Omega \psi \rangle \quad &&= e_1 + e_2, \\
\psi^2 &= \langle \Omega \otimes \Omega \psi \rangle &&= e_1 \otimes e_1 + e_2 \otimes e_2.
\end{aligned}$$

Here the M_1 model sees a single beam in the direction $e_1 + e_2$. But because ψ^2 does not have the moments of a single beam at $e_1 + e_2$ (these would be $(e_1 + e_2) \otimes (e_1 + e_2)$), the M_2 ansatz can distinguish these cases.

Remark 3 This problem could be circumvented by exploiting the linearity of the underlying kinetic equation (1-4). Indeed, suppose that for each i, ψ_i is the solution of (1) with the collision operator (2), (3) or (4) with a boundary condition $\psi|_{\partial Z} = \psi_{b_i}$, where ψ_{b_i} contains (for example) only a single i-th beam entering the domain, and an initial condition of zero. Then the solution of (1-4) with the boundary condition $\psi|_{\partial Z} = \sum_i \psi_{b_i}$ and the same initial condition would be $\sum_i \psi_i$. Each solution ψ_i can be approximated by solving the M_N system (5) with the associated collision operator. This way one obtains an approximation of the solution $\sum_i \psi_i$ with multiple beams by solving the M_N system for each beam separately.

3 Approximation of the M_2 closure

The computation of the M_2 closure in three dimensions of space cannot be simplified to one dimension by using symmetry arguments as in the M_1 case (Section 2.3), therefore typically it would be computed by numerically solving the minimization problem (12). However, this method would be too expensive for the applications we have in mind, so we propose an approximation which takes advantage of the underlying hierarchical structure of the closure and is exact for certain special boundary cases.

A naive idea to approximate the M_2 closure consists in solving (12) for a large amount of values of (ψ^0, ψ^1, ψ^2) and directly constructing a polynomial fitting those values. Such an approximation is not very satisfactory as it does not satisfy basic properties. For instance, when choosing a 1D function $\psi(\Omega_1)$, the closure ψ^3 should be the third order moment of a 1D distribution $\psi_R(\Omega_1)$. This would not be enforced by such a naive polynomial approximation.

Instead we propose the following: First we use the same method as in Section 2.3, to approximate the closure ψ^3 in the M_1 case. Then we extend this progressively to more general cases until obtaining an approximation of the general M_2 closure.

In the first subsection, we introduce the realizability domain for the M_2 model, which is the domain of physically relevant moments. In the second subsection, an approximation of the closure is proposed in some subsets of the realizability domain. In the third subsection, a polynomial fit is proposed which is correct in these subsets. Finally, we consider the properties of the obtained approximation.

3.1 The realizability domain for the M_2 model

The solution of the kinetic equation (1-4) is positive. This implies that its moments $\langle(1, \Omega, \Omega\otimes\Omega)\psi\rangle$ evolve in the realizability domain $\mathscr{R}_2 \subset \mathbb{R}\times\mathbb{R}^3\times\mathbb{R}^{3\times3}$ (defined in (11)). The solution of the moment system (5-8) with the M_2 closure needs to be inside this set. Indeed the M_2 closure exists only if there exists an ansatz of the form (10) whose moments are (ψ^0, ψ^1, ψ^2). For moments on the unit sphere S^2, this is equivalent (according to Theorem 1) to requiring $(\psi^0, \psi^1, \psi^2) \in \mathscr{R}_2$.

The realizability domain $\mathscr{R}_2$ for moments of order up to 2 is characterized as follows.

Proposition 1 *The realizability domain for second order moments can be written*

$$\begin{aligned}\mathscr{R}_2 = \big\{(\psi^0, \psi^1, \psi^2) \in \mathbb{R}\times\mathbb{R}^3\times\mathbb{R}^{3\times3}, \quad s.t. \quad tr(\psi^2) = \psi^0 > 0 \\ \text{and} \quad \psi^0\psi^2 - \psi^1\otimes\psi^1 \text{is symmetric positive definite (s.p.d.)}\big\}.\end{aligned} \tag{16}$$

Proof This results follows directly from [31] which provided the following result

$$\begin{aligned}\bar{\mathscr{R}}_2 = \big\{(\psi^0, \psi^1, \psi^2) \in \mathbb{R}\times\mathbb{R}^3\times\mathbb{R}^{3\times3}, \quad \text{s.t.} \quad tr(\psi^2) = \psi^0 \geq 0 \\ \text{and} \quad \psi^0\psi^2 - \psi^1\otimes\psi^1 \text{is symmetric non-negative}\big\}.\end{aligned}$$

Then, using Theorem 1, one obtains the existence of a positive (instead of non-negative for the previous characterization) representing distribution for all moments $(\psi^0, \psi^1, \psi^2) \in int(\mathscr{R}_2)$ in the interior of the realizability domain. (16) is a characterization of this interior. Finally, by replacing one of the inequality in (16) by an equality, one can prove that there is no strictly positive representing distribution for such moments (see e.g. [15,16]), which prove the equality (16).

In order to simplify the computation of ψ^3, we use a transformation of the realizability domain. It consists of a normalization and a rotation.

Notation 1

- *N^i is the i-th moment normalized by the zeroth-order moment, i.e.*

$$N^i := \frac{\psi^i}{\psi^0}.$$

- *Let R be the rotation matrix that diagonalizes $\psi^0\psi^2 - \psi^1 \otimes \psi^1$. This also diagonalizes $N^2 - N^1 \otimes N^1$.*
- *$\mathscr{R}_T$ is the set of realizable moments after these transformations (rotation and normalization)*

$$\mathscr{R}_T := \left\{(N^1, N^2), \quad s.t. \quad tr(N^2) = 1 \quad and \quad N^2 - N^1 \otimes N^1 diagonal\ positive\right\}.$$

One passes easily from one set to the other

$$\mathscr{R}_2 \ni \left(\psi^0, \psi^1, \psi^2\right) = \left(\psi^0, \psi^0 R.N^1, \psi^0 R.N^2.R^T\right), \quad \text{with} \quad (N^1, N^2) \in \mathscr{R}_T. \tag{17}$$

Similarly, applying this transformation to ψ^3 yields

$$\psi^3 = \psi^0 Rot_3(R, N^3), \qquad Rot_3(R, N^3) = \sum_{i'=1}^{3}\sum_{j'=1}^{3}\sum_{k'=1}^{3} R_{i,i'}R_{j,j'}R_{k,k'}N^3_{i',j',k'}, \tag{18}$$

where $Rot_3(R, N^3)$ is the tensor N^3 rotated using the matrix R. After transformation, N^3 only depends on $(N^1, N^2) \in \mathscr{R}_T$.

Notation 2 *For $(N^1, N^2) \in \mathscr{R}_T$, as $tr(N^2) = 1$ we have*

$$tr(N^2 - N^1 \otimes N^1) = 1 - ||N^1||_2^2.$$

One can rewrite

$$N^2 = N^1 \otimes N^1 + (1 - ||N^1||_2^2) Diag(\gamma_1, \gamma_2, 1 - \gamma_1 - \gamma_2).$$

Then we can parametrize $\mathscr{R}_T$ by

$$\mathscr{R}_P = \left\{(N^1, \gamma_1, \gamma_2) \in B(0_{\mathbb{R}^3}, 1) \times]0, 1[\times]0, 1 - \gamma_1[\right\}.$$

In the next subsection, we exhibit values of N^3 in subsets of $\mathscr{R}_P$.

3.2 Special values of the closure

Now we define a hierarchy of subdomains of $\mathscr{R}_T$ and compute N^3 in each of them. Then we recall results about the boundary of $\mathscr{R}_T$.

3.2.1 N^3 in subdomains of $\mathscr{R}_T$

First we consider the relation between moments $(N^1, N^2) \in \mathscr{R}_T$ and functions of the form (10) and vice versa. From these relations, we can give the form of the closure N^3 in certain subsets of $\mathscr{R}_T$.

Notation 3 *We use the following monomial basis for polynomials up to degree two over the unit sphere*

$$\bar{m}(\Omega) = \left(\Omega_1, \quad \Omega_2, \quad \Omega_3, \quad \Omega_1^2, \quad \Omega_2^2, \quad \Omega_3^2, \quad \Omega_1\Omega_2, \quad \Omega_1\Omega_3, \quad \Omega_2\Omega_3\right),$$

and we write

$$\psi_R(\Omega) = \exp\left(\bar{\lambda}.\bar{m}(\Omega)\right), \tag{19}$$

with $\bar{\lambda} \in \mathbb{R}^9$.

Using Theorem 1, there exists a bijection between the Lagrange multipliers $\bar{\lambda} \in \mathbb{R}^9$ and the moments $(\psi^0, \psi^1, \psi^2) \in int(\mathscr{R}_2)$ in the interior of the realizability domain (remark that this interior is $int(\mathscr{R}_2) = \mathscr{R}_2$, see (16)). We consider the following hierarchy of subdomains of $\mathbb{R}^9$

$$\mathscr{L}_1 := \left\{(\lambda_1, 0, 0, \lambda_4, \lambda_5, \lambda_6, 0, 0, 0), \quad \text{s.t.} \quad (\lambda_1, \lambda_4, \lambda_5, \lambda_6) \in \mathbb{R}^4\right\} \subset \mathbb{R}^9, \tag{20a}$$

$$\mathscr{L}_2 := \left\{(\lambda_1, 0, 0, \lambda_4, \lambda_5, \lambda_5, 0, 0, 0), \quad \text{s.t.} \quad (\lambda_1, \lambda_4, \lambda_5) \in \mathbb{R}^3\right\} \subset \mathscr{L}_1, \tag{20b}$$

$$\mathscr{L}_3 := \left\{(\lambda_1, 0, 0, \lambda_4, \lambda_4, \lambda_4, 0, 0, 0), \quad \text{s.t.} \quad (\lambda_1, \lambda_4) \in \mathbb{R}^2\right\} \subset \mathscr{L}_2. \tag{20c}$$

Choosing $\bar{\lambda}$ in one of those sets in (19) gives ansätze ψ_R of the form

$$\psi_1(\Omega) = \exp(\lambda_1\Omega_1 + \lambda_4\Omega_1^2 + \lambda_5\Omega_2^2 + \lambda_6\Omega_3^2), \tag{21a}$$

$$\psi_2(\Omega) = \exp(\lambda_5 + \lambda_1\Omega_1 + (\lambda_4 - \lambda_5)\Omega_1^2), \tag{21b}$$

$$\psi_3(\Omega) = \exp(\lambda_4 + \lambda_1\Omega_1) \tag{21c}$$

respectively.

Definition 2 We denote by H^i the set of normalized and rotated moments of functions of the form (21):

$$H^i := \left\{\left\langle(\Omega, \Omega\otimes\Omega)\exp(\bar{\lambda}.\bar{m}(\Omega))\right\rangle, \quad \bar{\lambda} \in \mathscr{L}_i\right\} \cap \mathscr{R}_T. \tag{22}$$

Remark 4 Choosing the sets $\mathscr{L}_3 \subset \mathscr{L}_2 \subset \mathscr{L}_1 \subset \mathbb{R}^9$ was motivated by two reason. First the hierarchical character of these sets is necessary to the construction of the expansion of N^3 described in the next section. Second each scale of this hierarchy corresponds to a particular type of problems:

- H^1 corresponds to the case where ψ^1 is an eigenvector of ψ^2 (see computations in Appendix A.1).
- H^2 corresponds to a 1D problem. Indeed, one can see that the distribution (21b) depends only on one scalar Ω_1.
- H^3 corresponds to a first-order model (i.e. M_1 model). Indeed, one can see that the distribution (21c) corresponds to a distribution function obtained using a first-order model (i.e. when working with (ψ^0, ψ^1)).

In order to illustrate this hierarchy, possible distribution functions associated to each of those sets are depicted in Fig. 1, 2, 3, 4, 5 and 6. On those plots, the color on the unit sphere corresponds to the value of the distribution function (where blue corresponds to the lowest value and red the highest) given in (21). As H^3 and H^2 are related to 1D distribution, those distributions can be represented along the preferred axis, i.e. ψ_R in (21a) and (21b) as a function of Ω_1. Computing the moments of order one and two of the functions (21) reads

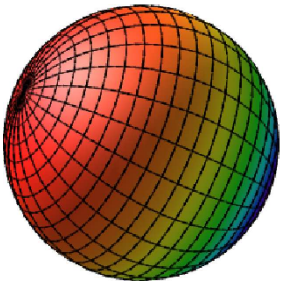

Fig. 1 Unit sphere colored by a distribution function associated to a vector of H^3

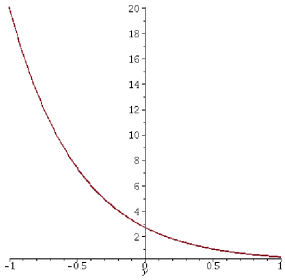

Fig. 2 Distribution function associated to a vector of H^3 along its preferred axis

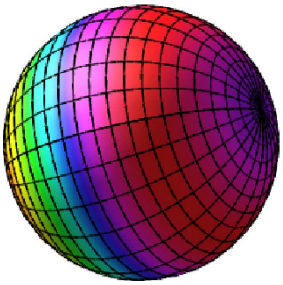

Fig. 3 Unit sphere colored by a distribution function associated to a vector of $H^2 \backslash H^3$

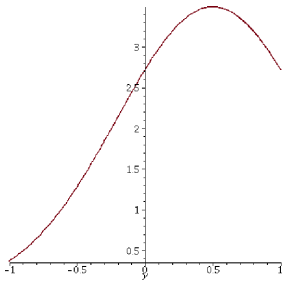

Fig. 4 Distribution function associated to a vector of $H^2 \backslash H^3$ along its preferred axis

$$\text{in } H^1, \quad N^1 = N_1^1 e_1, \quad N^2 = |N_1^1|^2 e_1 \otimes e_1 + (1 - |N_1^1|^2) Diag(\gamma_1, \gamma_2, 1 - \gamma_1 - \gamma_2), \tag{23a}$$

$$\text{in } H^2, \quad N^1 = N_1^1 e_1, \quad N^2 = |N_1^1|^2 e_1 \otimes e_1 + (1 - |N_1^1|^2) Diag(\gamma_1, \frac{1-\gamma_1}{2}, \frac{1-\gamma_1}{2}), \tag{23b}$$

$$\text{in } H^3, \quad N^1 = N_1^1 e_1, \quad N^2 = \frac{3\chi_2(|N_1^1|) - 1}{2} e_1 \otimes e_1 + \frac{1 - \chi_2(|N_1^1|)}{2} Id, \tag{23c}$$

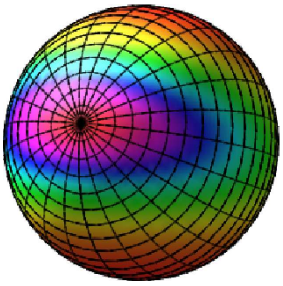

Fig. 5 Unit sphere colored by a distribution function associated to a vector of $H^1 \backslash H^2$

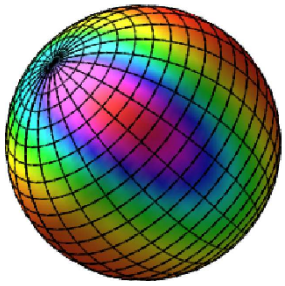

Fig. 6 Unit sphere colored by a distribution function associated to a vector of $\mathscr{R}_2 \backslash H^1$

where χ is the Eddington factor (see e.g. [33]). This leads to the following parametrization of H^i

$$
\begin{aligned}
(N^1,\gamma_1,\gamma_2) \in \mathscr{H}^1 &:= \left\{ (N^1,\gamma_1,\gamma_2) \in \mathscr{R}_P \quad \text{s.t.} \quad N^1 = N_1^1 e_1 \right\}, \\
(N^1,\gamma_1,\gamma_2) \in \mathscr{H}^2 &:= \left\{ (N^1,\gamma_1,\gamma_2) \in \mathscr{H}^1 \quad \text{s.t.} \quad \gamma_2 = \frac{1-\gamma_1}{2} \right\}, \\
(N^1,\gamma_1,\gamma_2) \in \mathscr{H}^3 &:= \left\{ (N^1,\gamma_1,\gamma_2) \in \mathscr{H}^2 \quad \text{s.t.} \quad \gamma_1 = \frac{\chi_2(|N_1^1|) - |N_1^1|^2}{1-|N_1^1|^2} \right\}.
\end{aligned}
$$

Similarly, computing the third-order moments of the distributions (21) reads

$$
\text{in } H^1, \quad N^3 = \kappa_2 1_{1,1,1} + \kappa_3 T_{1,2,2} + (N_1^1 - \kappa_2 - \kappa_3) T_{1,3,3}, \tag{24a}
$$

$$
\text{in } H^2, \quad N^3 = \kappa_1 1_{1,1,1} + \frac{N_1^1 - \kappa_1}{2}(T_{1,2,2} + T_{1,3,3}), \tag{24b}
$$

$$
\text{in } H^3, \quad N^3 = \chi_3 1_{1,1,1} + \frac{N_1^1 - \chi_3}{2}(T_{1,2,2} + T_{1,3,3}), \tag{24c}
$$

$$
T_{i,j,j} = 1_{i,j,j} + 1_{j,i,j} + 1_{j,j,i}, \quad 1_{i,j,k} = e_i \otimes e_j \otimes e_k,
$$

where χ_3, κ_1, κ_2 and κ_3 are scalar coefficients depending on $(N_1^1,\gamma_1,\gamma_2)$ respectively in $\mathscr{H}^3$ for χ_3, $\mathscr{H}^2$ for κ_1, and $\mathscr{H}^1$ for κ_2 and κ_3.

3.2.2 Limits of N^3 on the boundary of $\mathscr{R}_T$

The boundary of $\mathscr{R}_T$ is characterized by

$$
N^2 - N^1 \otimes N^1 \text{ has a zero eigenvalue.} \tag{25}
$$

At the boundary, the problem (12) has no solution (see e.g. [28,8]). However, we can deduce the following two results, first on the boundary of H^1 and then in the particular case when $||N^1||_2 = 1$, which we will use in the next subsection.

Proposition 2 *Suppose $(N^1,N^2) \in \partial H^1$, i.e. N^1 and N^2 is given by* (23a) *and*

$$
\exists V \in S^2, \quad \textit{s.t.} \quad V.\left(N^2 - N^1 \otimes N^1\right).V = 0, \tag{26}
$$

or equivalently $\gamma_1 = 0$, $\gamma_2 = 0$ or $1-\gamma_1-\gamma_2 = 0$ in (23a).

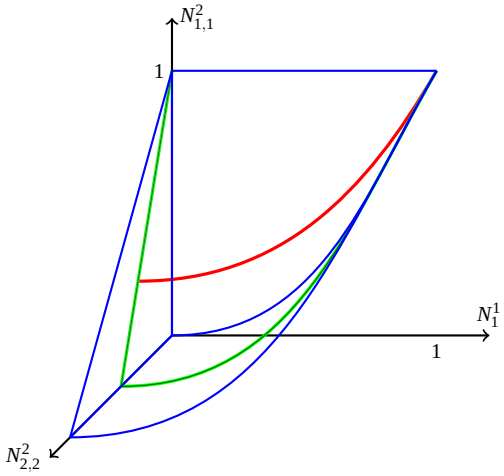

Fig. 7 Representation of H^3 (red line), H^2 (green plane) and H^1 (blue volume) in the space $(N^1_1, N^2_{1,1}, N^2_{2,2}) \in \mathbb{R}^3$.

Then the closure yields

$$N^3_{i,j,j} = N^1_i N^2_{j,j}, \quad N^3_{1,2,3} = 0. \tag{27}$$

Proof The moments in H^1 satisfy $N^2 = Diag(N^2_{1,1}, N^2_{2,2}, N^2_{3,3})$ and $N^1 = N^1_1 e_1$. Therefore the eigenvectors of $N^2 - N^1 \otimes N^1$ are the cartesian axis $V = e_i$.

This result follows from [31], where the author showed that the possible representing distributions $\psi_R(\Omega)$ for moments satisfying (26) are zero everywhere except on the line $\left\{\Omega \in S^2, \quad \text{s.t.} \quad (\Omega - N^1).V = 0\right\}$. Computing the following moments provides part of the equalities (27)

$$\int_{S^2} \Omega \otimes \Omega [(\Omega - N^1).V] \psi_R(\Omega) d\Omega = N^3.V - (N^1.V)N^2 = 0_{\mathbb{R}^{3\times 3}}.$$

The other equalities are simply obtained by remarking that some of the values of M_2 closure N^3 are zero when $(N^1, N^2) \in H^1$, e.g. using the eveness of (21a) according to Ω_2, one finds that $N^3_{2,2,2} = N^3_{2,3,3} = N^3_{1,2,3} = 0$. As the M_2 closure is a continuous function of N^1 and N^2, one retreives those zeros of N^3 on the boundary ∂H^1.

Fig. 7 depicts the hierarchy $H^3 \subset H^2 \subset H^1$ and its boundary in the space $(N^1_1, N^2_{1,1}, N^2_{2,2}) \in \mathbb{R}^3$ (these three components are indeed sufficient to parametrize H^1). H^3 is the red line included in H^2 the green plane, itself included in H^1 the blue volume.

Proposition 3 ([31]) *Suppose* $(N^1, N^2) \in \partial \mathscr{R}_T$, *such that* $||N^1||_2 = 1$, *then*

$$N^2 = N^1 \otimes N^1,$$

and the closure yields

$$N^3_{i,j,k} = N^1_i N^1_j N^1_k. \tag{28}$$

3.3 Approximation of the M_2 closure: the expansion

We first start by approximating N^3 in the set H^3. Then we extend it progressively into H^2, H^1, and finally $\mathscr{R}_2$.

The approximation is based on polynomial interpolations. For convenience, we introduce the following notation

Notation 4 *The polynomial of degree two interpolating the values A, B and C at the points a, b and c is denoted E, and Z denotes the polynomial of degree three which is zero in a, b and c:*

$$E\left((A,a),(B,b),(C,c)\right)(x) := A\frac{x-b}{a-b}\frac{x-c}{a-c} + B\frac{x-a}{b-a}\frac{x-c}{b-c} + C\frac{x-a}{c-a}\frac{x-b}{c-b},$$
$$Z\left(a,b,c\right)(x) := (x-a)(x-b)(x-c).$$

The hyperbolicity and the realizability properties (see Subsection 2.2) are considered at each step of the construction of approximated closure. The realizability, the hyperbolicity and the precision of the approximated closure are finally studied in the next subsection.

3.3.1 Initialization: the closure in H^3

First, one needs to approximate the Eddington factor χ_2 to compute the M_1 closure (15). As in the characterization of (16), the moments (ψ^0,ψ^1) are the moments of a positive function if and only if ([31])

$$\frac{||\psi^1||_2}{\psi^0} < 1.$$

Similarly using (16), simple computations show that (ψ^0,ψ^1,ψ^2), where ψ^2 has the form (15), are the moments of a positive function if and only if

$$x^2 < \chi_2(x) \leq 1, \quad \text{for } x \in [0,1[.$$

In order to construct a realizable closure (see Remark 2), we propose to approximate χ_2 by the convex combination

$$\chi_2(x) \approx x^2\theta_1(x) + (1-\theta_1(x))1.$$

The coefficient θ_1 is chosen to be an even function of x so that $\theta_1(x) \in [0,1]$ and the following exact value of the Eddington factor χ_2 and its derivative are satisfied on the boundary of the realizability domain (i.e. at $x=1$) and for the isotropic case (i.e. in $x=0$). The choice of fixing the exact values of the derivative χ_2' is motivated by the hyperbolic character of the M_2 closure (see the "hyperbolicity" paragraphs of Subsections 2.2 and 3.4). Those values are obtained by rewriting

$$\chi_2(|N^1|) = \frac{\left\langle \Omega_1^2 \exp(\alpha(|N^1|)\Omega_1)\right\rangle}{\langle \exp(\alpha(|N^1|)\Omega_1)\rangle}, \quad \chi_2'(|N^1|) = \frac{d\alpha}{d|N^1|}\frac{d}{d\alpha}\frac{\left\langle \Omega_1^2 \exp(\alpha(|N^1|)\Omega_1)\right\rangle}{\langle \exp(\alpha(|N^1|)\Omega_1)\rangle},$$

where $\frac{d\alpha}{d|N^1|} = \left(\frac{d|N^1|}{d\alpha}\right)^{-1}$. Then one can remark that

$$|N^1|(\alpha=0) = 0, \quad \lim_{\alpha\to+\infty}|N^1| = 1,$$

and since $|N^1|$ is a bijection of α (Theorem 1), this implies that

$$\alpha(|N^1| = 0) = 0, \quad \lim_{|N^1|\to 1} \alpha = +\infty,$$

then computing χ_2 and its derivative at those values using a symbolic computation software such as Maple$^{\text{TM}}$ ([38]) leads to

$$\chi_2(1) = 1, \quad \chi_2(0) = \frac{1}{3}, \quad \chi_2'(1) = 2, \quad \chi_2'(0) = 0. \tag{29}$$

In the end, we chose

$$\theta_1(x) = x^2 + \frac{2}{3}(1-x^2) + x^2(1-x^2)\left(c_0 + c_1x^2 + c_2x^4\right),$$

where the coefficients c_i are fitted to approximate the exact χ_2 for 10^3 values of x equally distributed in $[0,1]$ using Maple$^{\text{TM}}$ ([38]): $c_0 = -0.0954823981432433$, $c_1 = 0.229069986304953$ and $c_2 = -0.0344846229504588$. One can check that $\theta_1(x) \in [0,1]$ for all $x \in [-1,1]$.

Based on this approximation, one can construct a realizable closure in H^3. Using [31] again, a vector of 1D moments $(N^1_1, N^2_{1,1}, N^3_{1,1,1})$ is realizable if and only if

$$b_-(N^1_1, N^2_{1,1}) < N^3_{1,1,1} < b_+(N^1_1, N^2_{1,1}),$$
$$b_-(N^1_1, N^2_{1,1}) := -N^2_{1,1} + \frac{(N^1_1+N^2_{1,1})^2}{(1+N^1_1)}, \quad b_+(N^1_1, N^2_{1,1}) := N^2_{1,1} - \frac{(N^1_1-N^2_{1,1})^2}{(1-N^1_1)}.$$

Then similarly to above, we construct a realizable closure in H^3 as a convex combination (see Remark 2)

$$\chi_3(x) = b_-(x, \chi_2(x))\theta_2(x) + b_+(x, \chi_2(x))(1-\theta_2(x)).$$

The coefficient θ_2 is chosen so that $\theta_2(x) \in [0,1]$, such that χ_3 is odd and the following exact value of χ_3 and its derivative are satisfied, on the boundary of the realizability domain (i.e. at $x = 1$) and for the isotropic case (i.e. at $x = 0$)

$$\chi_3(1) = 1, \quad \chi_3(0) = 0, \quad \chi_3'(1) = 3, \quad \chi_3'(0) = \tfrac{1}{2}.$$

Those values are obtained from the same method as for χ_2 in (29). In the end, we chose

$$\theta_2(x) = \frac{1}{2} + x\left(-\frac{1}{2} + (1-x^2)(d_0 + d_1x^2 + d_2x^4)\right),$$

where the coefficients d_i are fitted to approximate the exact χ_3 for 10^3 values of x equally distributed in $[0,1]$ using Maple$^{\text{TM}}$ ([38]): $d_0 = 0.386143553495150$, $d_1 = 0.488034553677475$ and $d_2 = -0.681343955348390$. One can check that $\theta_2(x) \in [0,1]$ for all $x \in [-1,1]$.

3.3.2 Extension to H^2 : the 1D approximated closure

Using the above results and the form of N^3 in (24b), we define an approximation of N^3 in H^2 by approximating κ_1 as follows

$$\kappa_1(x,y) = b_-(x,y)\theta_3(x,y) + b_+(x,y)(1-\theta_3(x,y)).$$

The coefficient θ_3 is chosen such that $\theta_3(x,y) \in [0,1]$ so that the resulting closure is realizable (see Remark 2). Furthermore it is chosen to have the exact value on the boundary of the realizability domain (i.e. when $(N^1,N^2) \in \partial H^2$ as in Proposition 2) and the approximated value in H^3 given above, that is

$$\kappa_1(N_1^1,0) = (N_1^1)^3, \quad \kappa_1\left(N_1^1, \frac{\chi_2(N_1^1) - |N_1^1|^2}{1-|N_1^1|^2}\right) = \chi_3(N_1^1), \quad \kappa_1(N_1^1,1) = N_1^1.$$

In the end, we chose

$$T_1 := \tfrac{b_+-\kappa_1}{b_+-b_-}(x,0), \quad T_2 := \tfrac{b_+-\kappa_1}{b_+-b_-}\left(x, \tfrac{\chi_2(x)-x^2}{1-x^2}\right), \quad T_3 := \tfrac{b_+-\kappa_1}{b_+-b_-}(x,1),$$
$$\theta_3(x,y) = E\left((T_1,0), \left(T_2, \tfrac{\chi_2(x)-x^2}{1-x^2}\right), (T_3,1)\right)(y) + Z\left(0, \tfrac{\chi_2(x)-x^2}{1-x^2}, 1\right)(y) Q_1(x,y),$$

where Q_1 is a polynomial of x and y of degree sixteen. Its coefficients are chosen such that the discrete L^2 distance between the approximated and the exact κ_1 (computed by solving (12) for 10^4 values of $(N^1,N^2) \in H^2$, given by 100 values of x equally distributed in $[0,1]$ and 100 of y equally distributed in $[0,1]$) is minimized. The degree of this polynomial approximation is chosen very high because a high precision is required for the next extension (i.e. to H^1 and then to $\mathscr{R}_T$). The discrete L^∞ error compared to the solution of the minimization problem (12) for those 10^4 values of $(N^1,N^2) \in H^2$ is 8.43×10^{-3}. Our polynomial satisfies $\theta_3(x,y) \in [0,1]$ for all $x \in [-1,1]$ and $y \in [0,1]$.

3.3.3 Extension to H^1

This procedure can be repeated to approximate N^3 in H^1.

Using Proposition 2 and the previous approximation, we aim to write an approximation of κ_2 and κ_3 (in (24a)) satisfying

$$\kappa_2(N_1^1,\gamma_1,0) = (N_1^1)^3 + N_1^1(1-|N_1^1|^2)\gamma_1, \qquad \kappa_2(N_1^1,\gamma_1,\frac{1-\gamma_1}{2}) = \kappa_1(N_1^1,\gamma_1),$$
$$\kappa_2(N_1^1,\gamma_1,1-\gamma_1) = (N_1^1)^3 + N_1^1(1-|N_1^1|^2)\gamma_1,$$
$$\kappa_3(N_1^1,\gamma_1,0) = 0, \qquad \kappa_3(N_1^1,\gamma_1,\frac{1-\gamma_1}{2}) = \frac{1}{2}\left(N_1^1 - \kappa_1(N_1^1,\gamma_1)\right),$$
$$\kappa_3(N_1^1,\gamma_1,1-\gamma_1) = (N_1^1)^3 + N_1^1(1-|N_1^1|^2)(1-\gamma_1).$$

Similarly to above, we propose an approximation of the form

$$\kappa_2(x,y,z) = E\left((\kappa_2(x,y,0),0), \left(\kappa_2(x,y,\frac{1-y}{2}), \frac{1-y}{2}\right), (\kappa_2(x,y,1-y),1-y), \right)(z)$$
$$+ Z\left(0, \frac{1-y}{2}, 1-y\right)(z) Q_2(x,y,z),$$
$$\kappa_3(x,y,z) = E\left((\kappa_3(x,y,0),0), \left(\kappa_3(x,y,\frac{1-y}{2}), \frac{1-y}{2}\right), (\kappa_3(x,y,1-y),1-y), \right)(z)$$
$$+ Z\left(0, \frac{1-y}{2}, 1-y\right)(z) Q_3(x,y,z),$$

where Q_2 and Q_3 are polynomials in x, y and z of degree eight. The coefficients of those polynomials are chosen such that the discrete L^2 distance between the approximated and the exact κ_2 and κ_3 (computed by solving (12) for 8×10^3 values of $(N^1,N^2)\in H^1$, given by 20 values of x equally distributed in $[0,1]$, and 20 values of y in $[0,1]$ and 20 of z in $[0,1-y]$) is minimized. The discrete L^∞ error compared to the solution of the minimization problem (12) for those 8×10^3 values of $(N^1,N^2)\in H^1$ is of $2.09.10^{-2}$.

3.3.4 Extension to the whole realizability domain $\mathscr{R}_T$

We now aim to extend this approximation to $\mathscr{R}_T$ which will provide us with an approximation of ψ^3 for any $(\psi^0,\psi^1,\psi^2)\in\mathscr{R}_2$ through (17). This last extension again consists of an interpolation.

The previous approximation provides a closure when N^1 is along one of the Cartesian axes. One can also compute the closure when $|N^1|=1$ through Proposition 3.

Now suppose we want to compute N^3 at the point $P_0=(N^1,N^2)\in\mathscr{R}_T$, parametrized by $(N^1,\gamma_1,\gamma_2)=(xe_1+ye_2+ze_3,\beta_1,\beta_2)$. Let us define the following points (see Fig. 8 and 9)

$$P_1\equiv(N^1,\gamma_1,\gamma_2)=(xe_1,\beta_1,\beta_2),\quad P_2\equiv(N^1,\gamma_1,\gamma_2)=(ye_2,\beta_1,\beta_2),$$
$$P_3\equiv(N^1,\gamma_1,\gamma_2)=(ze_3,\beta_1,\beta_2),$$

corresponding to projections of P_0 onto each Cartesian axis. At those points, N^1 is an eigenvalue of N^2. Then we can use the approximation techniques in H_1 of the previous paragraph (see remark 4). Now let us define the lines and points (see Fig. 8 and 9)

$$L_1=(P_1,P_0),\quad L_2=(P_2,P_0),\quad L_3=(P_3,P_0)$$
$$P_4=L_1\cap\{||N^1||_2=1\}\equiv(xe_1+a_1ye_2+a_1ze_3,\beta_1,\beta_2),\quad a_1=\sqrt{\tfrac{1-x^2}{y^2+z^2}},$$
$$P_5=L_2\cap\{||N^1||_2=1\}\equiv(a_2xe_1+ye_2+a_2ze_3,\beta_1,\beta_2),\quad a_2=\sqrt{\tfrac{1-y^2}{x^2+z^2}},$$
$$P_6=L_3\cap\{||N^1||_2=1\}\equiv(a_3xe_1+a_3ye_2+ze_3,\beta_1,\beta_2),\quad a_3=\sqrt{\tfrac{1-z^2}{x^2+y^2}}.$$

The closure N^3 is either known (at P_4, P_5 and P_6) or approximated (at P_1, P_2 and P_3) at each of those points. Thus for $(N^1,N^2)\in\mathscr{R}_T$ the different components of the closure N^3 are approximated by convex combinations of the values of N^3 computed or approximated at the points P_i for $i\in\{1,2,\dots6\}$. In particular, for $i\in\{1,2,3\}$, we approximate $N^3_{i,j,j}$ with a convex combination of its approximate value for P_i and its exact value for P_{3+i}. Similarly, the value of $N^3_{1,2,3}$ is known at the points $(N^1,\gamma_1,\gamma_2)=(0_{\mathbb{R}^3},\gamma_1,\gamma_2)$ and $(N^1,\gamma_1,\gamma_2)=(N^1/||N^1||_2,\gamma_1,\gamma_2)$, and we simply approximate it by a convex combination of the value at those points. In the

end, those approximations are

$$
\begin{aligned}
N^3_{1,1,1}(N^1,\gamma_1,\gamma_2) &\approx (1-\alpha_1)N^3_{1,1,1}(N^1_1 e_1,\gamma_1,\gamma_2)+\alpha_1 (N^1_1)^3,\\
N^3_{1,2,2}(N^1,\gamma_1,\gamma_2) &\approx (1-\alpha_1)N^3_{1,2,2}(N^1_1 e_1,\gamma_1,\gamma_2)+\alpha_1 N^1_1\beta_1^2|N^1_2|^2,\\
N^3_{1,3,3}(N^1,\gamma_1,\gamma_2) &\approx (1-\alpha_1)N^3_{1,3,3}(N^1_1 e_1,\gamma_1,\gamma_2)+\alpha_1 N^1_1\beta_1^2|N^1_3|^2,\\
\alpha_1 &= \frac{|N^1_2|^2+|N^1_3|^2}{1-|N^1_1|^2}, \quad \beta_1=\sqrt{\frac{1-|N^1_1|^2}{|N^1_2|^2+|N^1_3|^2}},\\
N^3_{1,1,2}(N^1,\gamma_1,\gamma_2) &\approx (1-\alpha_2)N^3_{1,1,2}(N^1_2 e_2,\gamma_1,\gamma_2)+\alpha_2 N^1_2\beta_2^2|N^1_1|^2,\\
N^3_{2,2,2}(N^1,\gamma_1,\gamma_2) &\approx (1-\alpha_2)N^3_{2,2,2}(N^1_2 e_2,\gamma_1,\gamma_2)+\alpha_2 (N^1_2)^3,\\
N^3_{2,3,3}(N^1,\gamma_1,\gamma_2) &\approx (1-\alpha_2)N^3_{2,3,3}(N^1_2 e_2,\gamma_1,\gamma_2)+\alpha_2 N^1_2\beta_2^2|N^1_3|^2,\\
\alpha_2 &= \frac{|N^1_1|^2+|N^1_3|^2}{1-|N^1_2|^2}, \quad \beta_2=\sqrt{\frac{1-|N^1_2|^2}{|N^1_1|^2+|N^1_3|^2}},\\
N^3_{1,1,3}(N^1,\gamma_1,\gamma_2) &\approx (1-\alpha_3)N^3_{1,1,3}(N^1_3 e_3,\gamma_1,\gamma_2)+\alpha_3 N^1_3\beta_3^2|N^1_1|^2,\\
N^3_{2,2,3}(N^1,\gamma_1,\gamma_2) &\approx (1-\alpha_3)N^3_{2,2,3}(N^1_3 e_3,\gamma_1,\gamma_2)+\alpha_3 N^1_3\beta_3^2|N^1_2|^2,\\
N^3_{3,3,3}(N^1,\gamma_1,\gamma_2) &\approx (1-\alpha_3)N^3_{3,3,3}(N^1_3 e_3,\gamma_1,\gamma_2)+\alpha_3 (N^1_3)^3,\\
\alpha_3 &= \frac{|N^1_1|^2+|N^1_2|^2}{1-|N^1_3|^2}, \quad \beta_3=\sqrt{\frac{1-|N^1_3|^2}{|N^1_1|^2+|N^1_2|^2}},\\
N^3_{1,2,3}(N^1,\gamma_1,\gamma_2) &\approx N^1_1 N^1_2 N^1_3.
\end{aligned}
$$

For $N^3_{1,2,3}$, several other linear combinations were possible, but we found that this simple expression gave the best approximation of the M_2 closure. The discrete L^∞ error compared to the solutions of the minimization problem (12) for 3.2×10^6 values of $(N^1,N^2)\in\mathscr{R}_T$ is of $3.12.10^{-2}$. Those values are obtained from 20 values of N^1_1 equally distributed in $[0,1]$, 20 of N^1_2 in $[0,\sqrt{1-|N^1_1|^2}]$, 20 of N^1_2 in $[0,\sqrt{1-|N^1_1|^2-|N^1_2|^2}]$, 20 of γ_1 in $[||N^1||_2^2,1]$ and 20 of γ_2 in $[0,1]$.

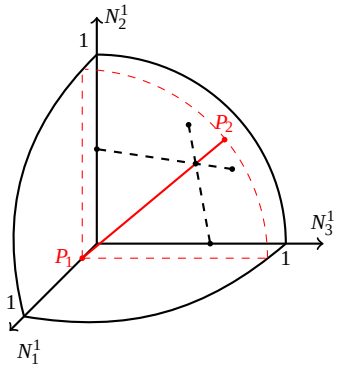

Fig. 8 Configuration at fixed N^2.

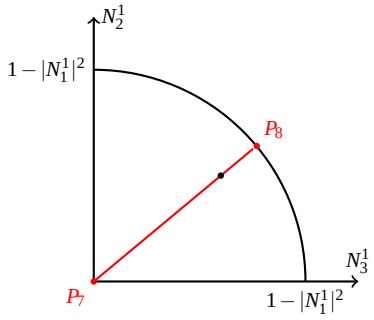

Fig. 9 Configuration at fixed N^2 and N^1_3.

3.4 Properties of the approximation

We study here the accuracy and the numerical cost to compute the approximated closure, the hyperbolicity and the realizability property with the approximated closure.

3.4.1 Precision and numerical cost

Our approach consists of a polynomial approximation. Evaluating the polynomials is very fast compared to solving the minimization problem (12), as the numerical methods generally require iterative algorithms. The approximate closure is compared to the one obtained by solving this minimization problem using the routines HUMSL of MINPACK [43] and DCUHRE from [5]. The routine HUMSL is based on an iterative algorithm using the gradient and the Hessian of ψ^3. The routine DCUHRE is an adaptive quadrature algorithm for functions of several variables. The precision for this minimization algorithm (both for the minimization and the quadrature) can be fixed. In order to have a fair comparison of computational times and precision, we first ran the code with high precision (L^∞ error of 10^{-9}) in order to have an accurate reference (it ran for 3h 33min), and then we ran it again with a precision equivalent to that of our approximation. We fixed the maximum number of iterations for both the quadrature and the minimization routine at 10^6 iterations, and we checked that this was not reached during the computations (meaning the desired precision was always obtained). Computing the approximation is much faster than solving the minimization problem with this method as shown in Table 1.

	Minimization solver	Approximation
Computation times	1654 sec = 27min 34sec	0.434 sec
L^∞ error	$< 3 \times 10^{-2}$	3.12×10^{-2}

Table 1 Comparing computation times for the closure with 3.2×10^6 points in $\mathscr{R}_T$ between the minimization solver and our approximation.

3.4.2 Hyperbolicity

It is well-known [34] that the M_2 system is a hyperbolic system of conservation laws, as long as $(\psi^0, \psi^1, \psi^2) \in \mathscr{R}_2$. This means that the Jacobian $\nabla_{(\psi^0,\psi^1,\psi^2)}(\psi^1, \psi^2, \psi^3)$ is diagonalizable with real eigenvalues. In this paragraph, we study the hyperbolicity of our approximation of the M_2 closure at each step of the expansion of the previous subsection, i.e. when (N^1, N^2) is in $\mathscr{H}^3$, $\mathscr{H}^2$, $\mathscr{H}^1$, and $\mathscr{R}_T$.

For the M_1 approximation, i.e. for moments in H^3, we can work in a reference frame in which $\psi^1 = ||\psi^1|| e_1$. Using this simple rotation, one can show that the Jacobian reduces into

$$\nabla_{(\psi^0,||\psi^1||_2)} \begin{pmatrix} ||\psi^1||_2 \\ \psi^0 \chi_2(\frac{||\psi^1||_2}{\psi^0}) \end{pmatrix} = \begin{pmatrix} 0 & 1 \\ \chi_2(\frac{||\psi^1||_2}{\psi^0}) - \frac{||\psi^1||}{\psi^0}\chi_2'(\frac{||\psi^1||_2}{\psi^0}) & \chi_2'(\frac{||\psi^1||}{\psi^0}) \end{pmatrix}.$$

This leads to the following requirement for hyperbolicity

$$\forall x \in [0,1], \quad \chi_2'(x) - 4(\chi_2(x) - x\chi_2'(x)) \geq 0,$$

which is satisfied by our approximation.

In H^2 (i.e. the 1D case), using the same method, one obtains the hyperbolicity if the following matrix is diagonalizable with real eigenvalues

$$\begin{pmatrix} 0 & 1 & 0 \\ 0 & 0 & 1 \\ N^3_{1,1,1} - N^1_1 \partial_{N^1_1} N^3_{1,1,1} - N^2_{1,1} \partial_{N^2_{1,1}} N^3_{1,1,1} & \partial_{N^1_1} N^3_{1,1,1} & \partial_{N^2_{1,1}} N^3_{1,1,1} \end{pmatrix}.$$

Studying the roots of the characteristic polynomial of this matrix (i.e. roots of a cubic function), one can verify that this matrix is indeed diagonalizable with real eigenvalues. This means that the M_2 system of equations for 1D problems with the approximated closure is hyperbolic.

In H^1 and in $\mathscr{R}_T$, the problem is 3D. The Jacobian can not be easily reduced into a smaller matrix, so the full Jacobian is studied. As studying moments in H^1 does not provide any simplification of the Jacobian compared to moments in $\mathscr{R}_T$, we directly study the hyperbolicity in the general case, for moments in $\mathscr{R}_T$. Checking that the eigenvalues of the full Jacobian $\nabla_{(\psi^0,\psi^1,\psi^2)}(\psi^1,\psi^2,\psi^3)$ are real for all $(N^1,N^2) \in \mathscr{R}_T$ is complicated, and we have not been to verify analytically that the eigenvalues are always real. Instead, we verified this property was satisfied for a finite number of points in $\mathscr{R}_T$, i.e. for 10^5 values of $(N^1,N^2) \in \mathscr{R}_T$. Those values are obtained from 10 values of N^1_1 equally distributed in $[0,1]$, 10 of N^1_2 in $[0,\sqrt{1-|N^1_1|^2}]$, 10 of N^1_2 in $[0,\sqrt{1-|N^1_1|^2-|N^1_2|^2}]$, 10 of γ_1 in $[||N^1||^2_2,1]$ and 10 of γ_2 in $[0,1]$.

Remark 5 Since solving the minimization problem (12) numerically also introduces errors, this may also result in a loss of hyperbolicity.

3.4.3 Realizability

For any set of realizable moments $(\psi^0,\psi^1,\psi^2) \in \mathscr{R}_2$, we have constructed a closure ψ^3. One may expect that the set of moments $(\psi^0,\psi^1,\psi^2,\psi^3) \in \mathscr{R}_3$ is also realizable, i.e. are the moments of one positive function. The realizability condition on ψ^3 in 1D (see e.g. [31,15]), i.e. in the particular case when $(\psi^0,\psi^1,\psi^2) \in H^2$, can easily be verified. In our framework, this condition can be rewritten (see Remark 2)

$$\theta_3 \in [0,1],$$

which is satisfied by our approximation. This means that the proposed closure is realizable when working with 1D problems. In multi-D, there is, to the authors' knowledge, no similar characterization of the realizability to check. As our approach approximates a realizable closure ψ^3 and has the right value in limit case when $(\psi^0,\psi^1,\psi^2) \in \partial\mathscr{R}_T$, we may expect the approximation to be realizable.

Remark 6 Numerically solving the minimization problem (12) introduces errors which may also result in a loss of realizability.

4 Numerical results

Now we compare the solutions computed with the M_1 and M_2 models (both with approximated closure and by using the minimization algorithm previously mentioned for (12)) to

those results obtained by solving the kinetic model directly on several test cases. First, the numerical approaches used to solve the kinetic and moment equations are described. Then the results for each test cases are presented. Those tests consist in computing the dose for given boundary conditions which correspond to: a single beam in 1D, two opposite beams in 1D, a single beam in 2D whose direction is not aligned with the mesh, two beams in 2D and finally a single beam in an inhomogeneous medium corresponding to a human chest.

4.1 Numerical approaches

In each test case, the moments results are compared to the results of a reference code.

In 1D, this reference code is a kinetic solver for (1). However, discretizing (1) directly with the LB operator (2) or CSD operator (3) is not efficient. Indeed the differential cross sections in (2) and (3) are very peaked, and such a discretization would require a meshgrid in angle and energy fine enough to represent those peaks. We could not afford to use such a fine mesh. For the same reason, the proposed moment solver is only used for the equations (5) with the CSD (7) or FP (8) operator. In 1D, the kinetic and moment solvers are based on the equation (1) and (5) with a FP operator (4) and (8).

In 1D, we also compared the results with the approximated closures to the one using the closure obtained by solving the minimization problem (12). This closure was obtained by using the routines "HUMSL" of MINPACK [43] and "DQAGS" of QUADPACK [47], using a maximum tolerance of 3.10^{-2} (equivalent to the precision as our approximation) and a maximum number of iterations of 100. For the purposes of dose calculation these routines provide an accurate M_N closure which is easy to incorporate into a numerical solver. However, for cases where the moments are closer to the boundary of realizability (and the optimization problem becomes numerically ill-conditioned) special techniques have been developed [27,2,1] which make the entropy closure problem tractable.

We used the Monte-Carlo solver PENELOPE ([20]) as reference. PENELOPE is one of the state-of-the-art codes for electron transport, and has been validated against experiments. Note that PENELOPE, when compared to our model, also takes into account more physical effects (like e.g. pair production and bremsstrahlung).

The numerical schemes are constructed as follows: Due to the integral in (4), in order to compute ψ at energy ε, one requires the knowledge of the value of ψ for all energies between ε and ε_{max}. In practice, we solve it from a maximum energy ε_{max} to zero.

The 1D kinetic equation is solved using an upwind scheme for the spatial and energy derivatives. The angular diffusion operator is discretized using a central scheme, and the integral operator with a midpoint quadrature rule.

The moment solver was obtained by adapting the relaxation approach proposed in [46] to the equations (5) with the collisions operators (8) and (7). For the sake of clarity, the numerical scheme for moment equations is written here for a 1D problem with a Fokker-Planck operator (8). It can be easily extended to 2D or 3D problems and to the CSD colllision operator (7). First let us rewrite the moment system 5 with the FP operator (8) under the form

$$\partial_x \bar{F}(\bar{\psi})(x,\varepsilon) = \rho(x)\left[\partial_\varepsilon(S\bar{\psi})(x,\varepsilon) - T(\varepsilon)\bar{\bar{A}}\bar{\psi}(x,\varepsilon') + \int_\varepsilon^{\varepsilon_{max}} \bar{\bar{\sigma}}(\varepsilon',\varepsilon)\bar{\psi}(x,\varepsilon')d\varepsilon'\right], \quad (30)$$

where $\bar{\psi}$ is a vector of moments and $\bar{F}(\bar{\psi})$ its associated flux; $\bar{\bar{\sigma}}$ is the matrix composed of the moments σ^i of the cross section; and $\bar{\bar{A}}$ is a matrix such that $\bar{\bar{A}}\bar{\psi}$ corresponds to the moments of the angular diffusion term, e.g. for M_1

$$\bar{\psi} = (\psi^0, \psi_1^1)^T, \quad \bar{F}(\bar{\psi}) = (\psi_1^1, \psi_{1,1}^2)^T, \quad \bar{\bar{\sigma}} = Diag(\sigma^0, \sigma^1), \quad \bar{\bar{A}} = Diag(0,2).$$

In the following, the subscript l corresponds to the spatial variable x_l and the superscript p to energy variable ε^p. In order not to be constrained by a Courant-Friedrichs-Lewy (CFL) condition which could be very restrictive for our problem (see e.g. [7,46]), we aim to construct an implicit numerical scheme. We propose the following scheme, which was obtained by discretizing in (30), the integral with a quadrature formula, the energy derivative with an Euler discretization and the spatial flux with an implicit form of HLL ([25]) scheme

$$\frac{\bar{F}(\bar{\psi})^p_{l+1}-\bar{F}(\bar{\psi})^p_{l-1}}{2\Delta x}-\frac{\bar{\psi}^p_{l-1}-2\bar{\psi}^p_l+\bar{\psi}^p_{l+1}}{2\Delta x}$$
$$+\rho_l\left[-\frac{(S\bar{\psi})^{p-1}_l-(S\bar{\psi})^p_l}{\Delta\varepsilon^p}+\left(T^p\bar{\bar{A}}-\bar{\bar{\sigma}}^{p,p}\Delta\varepsilon^p Id\right)\bar{\psi}^p_l-\sum_{p'=1}^{p-1}\bar{\bar{\sigma}}^{p',p}\bar{\psi}^{p'}_l\Delta\varepsilon^{p'}\right]=0.$$

This is an implicit equation for $\bar{\psi}^p$. We use an iterative solver inspired by [18], which consists of sweeping in the l variable. Let us write $\bar{\psi}^{p,k}_l$, the intermediate solution after sweeping k times. The solution is initialized by choosing $\bar{\psi}^{p,0}_l=\bar{\psi}^{p-1}_l$, then the following systems are solved iteratively: First

$$\frac{\bar{F}(\bar{\psi})^{p,k}_{l+1}-\bar{F}(\bar{\psi})^{p,k+1}_{l-1}}{2\Delta x}-\frac{\bar{\psi}^{p,k+1}_{l-1}-2\bar{\psi}^{p,k+1}_l+\bar{\psi}^{p,k}_{l+1}}{2\Delta x}$$
$$+\rho_l\left[-\frac{(S\bar{\psi})^{p-1}_l-(S\bar{\psi})^{p,k+1}_l}{\Delta\varepsilon^p}+\left(T^p\bar{\bar{A}}-\bar{\bar{\sigma}}^{p,p}\Delta\varepsilon^p Id\right)\bar{\psi}^{p,k+1}_l-\sum_{p'=1}^{p-1}\bar{\bar{\sigma}}^{p',p}\bar{\psi}^{p'}_l\Delta\varepsilon^{p'}\right]=0. \tag{31}$$

This corresponds to letting l run from 0 to l_{max} , i.e. from left to right, and implicitly using what has already been computed (i.e. $\bar{\psi}^{p,k+1}_{l-1}$) and explicitly using what is not (i.e. $\bar{\psi}^{p,k}_{l+1}$). Then we have l run from l_{max} to zero, i.e. from right to left

$$\frac{\bar{F}(\bar{\psi})^{p,k+1}_{l+1}-\bar{F}(\bar{\psi})^{p,k}_{l-1}}{2\Delta x}-\frac{\bar{\psi}^{p,k}_{l-1}-2\bar{\psi}^{p,k+1}_l+\bar{\psi}^{p,k+1}_{l+1}}{2\Delta x}$$
$$+\rho_l\left[-\frac{(S\bar{\psi})^{p-1}_l-(S\bar{\psi})^{p,k+1}_l}{\Delta\varepsilon^p}+\left(T^p\bar{\bar{A}}-\bar{\bar{\sigma}}^{p,p}\Delta\varepsilon^p Id\right)\bar{\psi}^{p,k+1}_l-\sum_{p'=1}^{p-1}\bar{\bar{\sigma}}^{p',p}\bar{\psi}^{p'}_l\Delta\varepsilon^{p'}\right]=0. \tag{32}$$

Equations (31) and (32) are solved iteratively until reaching a converged state, i.e. until k satisfies

$$\frac{\|\bar{\psi}^{p,k+1}_l-\bar{\psi}^{p,k}_l\|}{\|\bar{\psi}^{p,k}_l\|}<r$$

for all l, and for a chosen maximum residual r. In practice, we chose $r=10^{-1}$, and a minimum number of iterations k of 3.

The function of interest for medical physicists is the dose given by

$$D(x)=\int_0^{\varepsilon_{\max}}S(\varepsilon)\psi^0(x,\varepsilon)d\varepsilon.$$

For each test case we compute the dose produced by beams of electrons prescribed on the boundary of the medium by

$$\text{for}\quad \Omega.n<0,\quad \psi(x,\varepsilon,\Omega)=10^{10}\exp\left(-c_e(\varepsilon_0-\varepsilon)^2\right)\exp\left(-c_o(1-\Omega_p.\Omega)^2\right), \tag{33}$$

where ε_0, Ω_p are the energy and direction, respectively, of the prescribed beam, and n is a vector normal to the boundary in the outgoing direction.

If no beam is applied on one boundary we apply a zero distribution and assume that all particles injected at the other borders are stopped inside the medium.

The boundary conditions for the moment systems are defined by extracting moments from these boundary conditions.

The following test cases provide qualitative analysis of the approximation of the M_2 closure. Further analysis of the numerical schemes for moments and quantitative study (convergence results) will be provided in another paper. In all test cases, we used mesh cells $\Delta x = 0.01$ cm and 100 cells in energy, with a tolerance $r = 10^{-1}$ in the scheme for moments models. This precision was sufficient to observe the considered phenomena.

4.2 Simple beam in 1D

In this test case a 6 cm long uniform water phantom is irradiated with a beam of electrons. This is modelled with fixed $\rho = 1$ and boundary conditions (33)

$$\text{at} \quad x = 0\ cm: \qquad \varepsilon_0 = 10\ MeV, \quad \Omega_p = e_1, \quad c_e = 200 \quad \text{and} \quad c_o = 10^3.$$

The domain was meshed with 600 cells in position and 100 cells in energy.

For this test case, we normalize the dose by the quantity of injected particles, i.e.

$$\psi_i = \int_{\Omega_1 > 0} \int_0^{\varepsilon_{\max}} \psi(0, \varepsilon, \Omega) d\varepsilon d\Omega.$$

The doses obtained with the kinetic solver, the M_1 and M_2 solver with the closures obtained from the minimization procedure and approximations are represented on Fig. 10, and the computation times for this test case are gathered in Table 2. This simple case shows that

Model	Kinetic	minimization M_1	minimization M_2	approximated M_1	approximated M_2
Times	43.76 sec	4.58 sec	8.84 sec	0.016 sec	0.047 sec

Table 2 Computation times with the different models for the simple 10 MeV beam test case in 1D

the M_N models have the same qualitative behaviour as the kinetic reference. The dose obtained with the M_1 model is however imprecise. Its derivative is too high at the entry and raised slowly and gradually until reaching its maximum, while the dose obtained with the M_2 and the kinetic models have a lower derivative at the entry, a higher maximum, and faster decrease after the maximum. These differences are due to the error produced when approximating the kinetic solution of (1) by a M_N ansatz, as described in Section 2.4, but the results of the M_2 model already follow the kinetic reference with good precision.

The approximations of the M_1 and the M_2 closures give good agreement with the closure obtained from the minimization procedure. The accuracy of the approximated closure is characterized by the errors on the doses gathered in Table 3. As described in Table 2, the approximations of the M_N closures significantly accelerate (by around 200 times) the computation compared to using a minimization solver, which are themselves faster (between 5 to 10 times faster) than the kinetic computations.

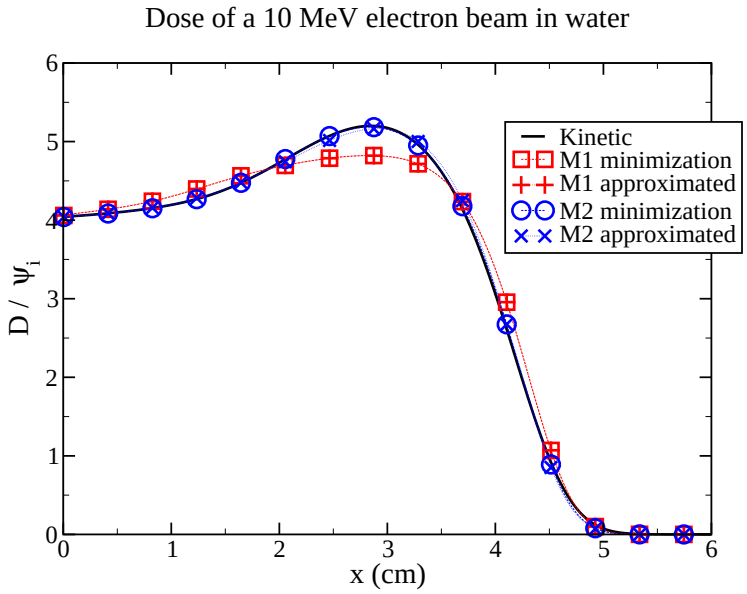

Fig. 10 Normalized dose produced by a 10 MeV electron beam in water using a kinetic, M_1 and M_2 solvers with the closures obtained from the minimization procedure and approximations.

	M_1 model	M_2 model
Discrete L^∞ error	$4.5.10^{-4}$	$1.75.10^{-2}$
Discrete L^2 error	$5.51.10^{-4}$	$1.62.10^{-2}$

Table 3 Discrete L^∞ and L^2 error between the doses obtained with the approximated and the minimization closure respectively for the M_1 and M_2 models.

4.3 Double beam in 1D

The multi-beam instability in 1D is studied through this test case (see Section 2.4): Two beams of same energy and intensity but with opposite direction are prescribed on both ends of a 8 cm long homogeneous water phantom, characterized by (33) with

$$\begin{aligned} &\text{at} \quad x = 0\ cm: \quad \varepsilon_0 = 10\ MeV, \quad \Omega_p = e_1, \quad c_e = 200 \quad \text{and} \quad c_o = 10^3; \\ &\text{at} \quad x = 8\ cm: \quad \varepsilon_0 = 10\ MeV, \quad \Omega_p = -e_1, \quad c_e = 200 \quad \text{and} \quad c_o = 10^3. \end{aligned}$$

The domain was meshed with 800 cells in position and 100 cells in energy.

The dose normalized by ψ_i obtained with the Monte-Carlo solver, and the M_1, M_2, double-M_1 (i.e. computing the dose of each beam seperately with M_1) and double-M_2 models is given on Fig. 11, and the computational times are presented in Table 4. The dose with the double M_N model was simply obtained from the dose of the previous test case by summing $D(x)+D(8\ cm-x)$ (see Remark 3). As described in [27], when using a M_N model for this problem, a shock appears in the middle of the medium. For M_1 this gives a high dose peak in the center of the medium, and for M_2 by a significantly smaller drop. It has been observed in [27] that the higher is the order of model, the smaller this shock becomes.

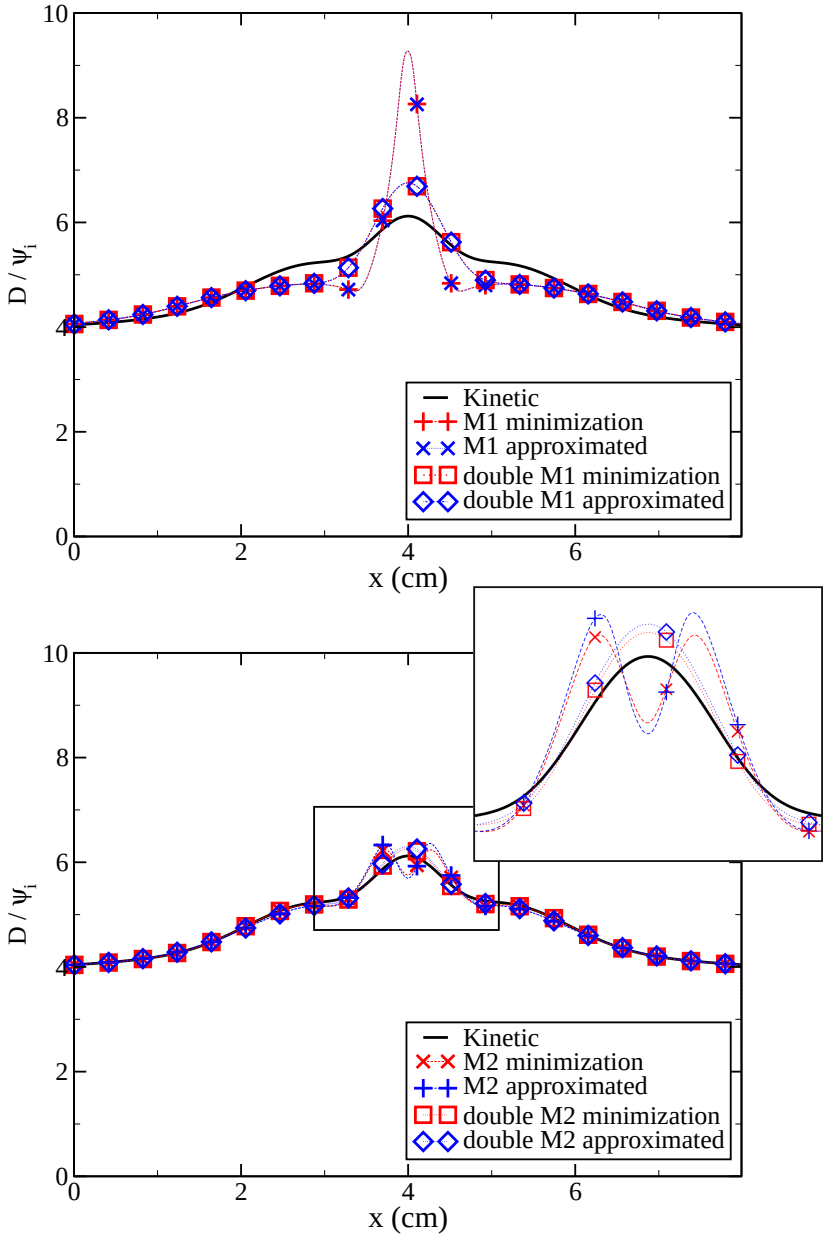

Fig. 11 Normalized dose produced by two 10 MeV electron beams in water using kinetic, M_1 and M_2 solvers with the closures obtained from the minimization procedure and approximations.

This artificial shock does not appear when considering the two beams separately. Through this case, we see that the non-physical effects of the angular approximation are smaller as

Model	Kinetic	minimization M_1	minimization M_2	approximated M_1	approximated M_2
Times	58.3 sec	7.81 sec	14.35 sec	0.023 sec	0.072 sec

Table 4 Computation times with the different models for the double 10 MeV beam test case in 1D

the order of the model raises. Similarly to the previous case, the M_2 results are close to the kinetic reference, except in the middle of medium, while the M_1 results are less precise. Finally the double-M_N models gives satisfactory results when high precision is required.

The accuracy of the approximations of the closures of the M_1, M_2, double M_1 and double M_2 models is characterized by the errors on the doses gathered in Table 5.

	M_1 model	M_2 model	double M_1 model	double M_2 model
Discrete L^∞ error	$5.00.10^{-4}$	$2.76.10^{-2}$	$4.50.10^{-4}$	$1.31.10^{-2}$
Discrete L^2 error	$6.59.10^{-4}$	$4.49.10^{-2}$	$6.44.10^{-4}$	$1.51.10^{-2}$

Table 5 Discrete L^∞ and L^2 error between the doses obtained with the approximated and the minimization closure respectively for the M_1, M_2, double M_1 and double M_2 models.

4.4 Simple inclined beam in 2D

In 2D, the computations need more computational power. We could not afford to use a minimization procedure in 2D to obtain the M_N closure, so only results using the approximated closures are presented.

This test consists of a beam of 10 MeV electrons in water, whose direction forms an angle of $\pi/3$ with the normal to the boundary. It is modeled by (33) with the parameters

$$\begin{aligned} &\text{at} \quad x = 0\ cm, \quad \text{for} \quad y \in [4.75\ cm, 5.25\ cm]: \\ &\quad \varepsilon_0 = 10\ MeV, \quad \Omega_p = \tfrac{\sqrt{3}e_1 - e_2}{2}, \quad c_e = 200 \quad \text{and} \quad c_o = 10^3. \end{aligned}$$

In order to compare our results with those of PENELOPE Monte-Carlo code, the dose is normalized by the maximum dose, i.e. we computed the percentage depth dose (PDD)

$$PDD(x) = \frac{D(x)}{\max(D)}.$$

The domain was meshed with 600×600 cells in position and 100 cells in energy.

The doses obtained with the different models are given on Fig. 12, and the computation times for that test case are given in Table 6. As for the 1D case, we observe that M_1 model

Model	Monte-Carlo	approximated M_1	approximated M_2
Computation times	$\approx$ 14 h	298 sec $\approx$ 5 min	868 sec $\approx$ 14 min

Table 6 Computation times with the different models for the simple 10 MeV beam test case in 2D

is overly diffusive. However, the effect in multi-D is lower than in 1D. The M_2 results are

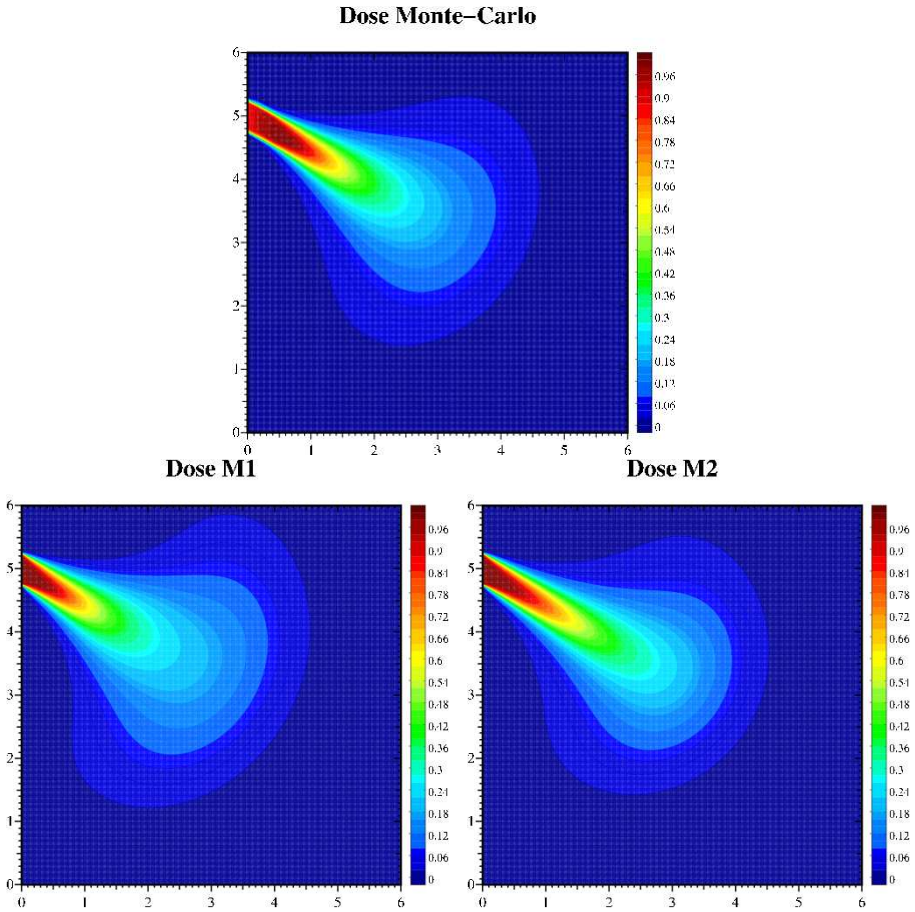

Fig. 12 Dose produced by a 10 MeV electron beam in water using the PENELOPE Monte-Carlo solver (top) and the M_1 (below left) and M_2 (below right) solvers using the approximated closures.

closer to the ones of the Monte-Carlo reference, one can remark that it is also somewhat overly diffusive.

The absolute errors between the doses obtained with the PENELOPE Monte-Carlo solver and the approximated M_1 and M_2 models are represented on Fig. 13.

The maximum error in the dose when using the approximated M_1 or M_2 model compared to the reference Monte-Carlo results are located at the entry of the medium and on both sides of the beam, and, when using the approximated M_1 model, in the middle of the beam between 1 and 2 cm depth.

4.5 Double beam in 2D

A 2D version of the test case 4.3 is now studied. It consists of two beams crossing each other with at an angle of $\pi/2$. As described in Section 2.4, M_1 model is known to fail to represent this phenomenon (also in 2D).

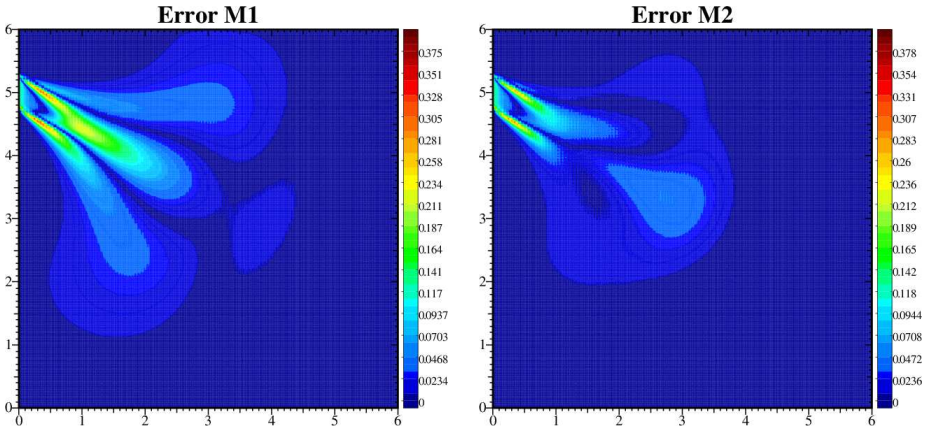

Fig. 13 Absolute error between the normalized doses obtained with Monte-Carlo solver and the M_1 (left) and M_2 (right) solvers using the approximated closures.

The beams are modelled by (33) with

$$\begin{aligned}
&\text{for} \quad x = 0\ cm, \quad y \in [0.75\ cm, 1.25\ cm]: \\
&\quad \varepsilon_0 = 10\ MeV, \quad \Omega_p = e_1, \quad c_e = 200 \qquad \text{and} \quad c_o = 10^3; \\
&\text{for} \quad y = 0\ cm, \quad x \in [0.75\ cm, 1.25\ cm]: \\
&\quad \varepsilon_0 = 10\ MeV, \quad \Omega_p = e_2, \quad c_e = 200 \qquad \text{and} \quad c_o = 10^3.
\end{aligned}$$

The same mesh as the previous case was used (i.e. 100 cells in energy and 600×600 cells in position), so the computation times for this case are identical to the previous one (see Table 6). The dose obtained with the different models are represented on Fig. 14. As expected, when using the M_1 model, the two incoming beams turn into one of direction (e_1+e_2). This effect is artificial and is due to M_1 moments extraction. It does not appear when using the M_2 model. The dose obtained with the M_2 model is slightly more diffusive than the dose obtained with the Monte-Carlo solver.

The absolute errors between the doses obtained with the PENELOPE Monte-Carlo solver and the approximated M_1, M_2, double-M_1 and double-M_2 models are represented on Fig. 15.

With the M_2 model, no visible shock appears, in contrast to the 1D double beam case of Section 4.3. However, the M_2 model gives a dose slightly more diffused than that of the double-M_2 model. The dose as computed by the double-M_2 model is indeed very close to the Monte-Carlo reference.

As in 1D, the double-beam instability does not appear when using the double-M_N models.

4.6 Chest geometry

This last test case is a 2D simple beam case with a density ρ corresponding to the density of a human chest. Here we show that our approach is valid with more realistic geometries.

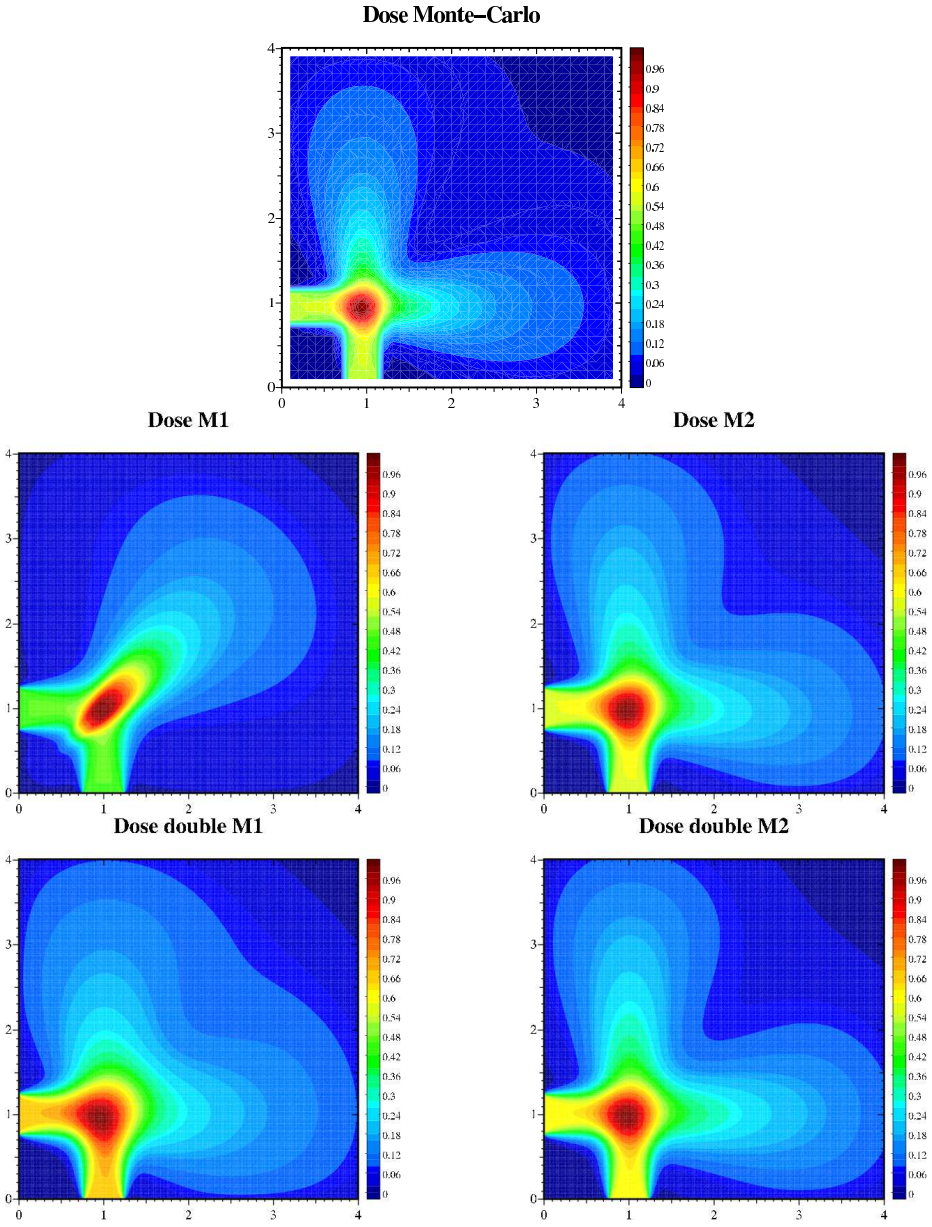

Fig. 14 Dose produced by two 10 MeV electron beams in water using the PENELOPE Monte-Carlo solver (top), a M_1 solver (middle left) and a M_2 solver (middle right), a double-M_1 solver (below left) and a double-M_2 solver (below right), with the approximated closures.

The domain is of size 21.825 cm $\times$ 37.5 cm meshed with 224 $\times$ 384 cells, and 100 cells in

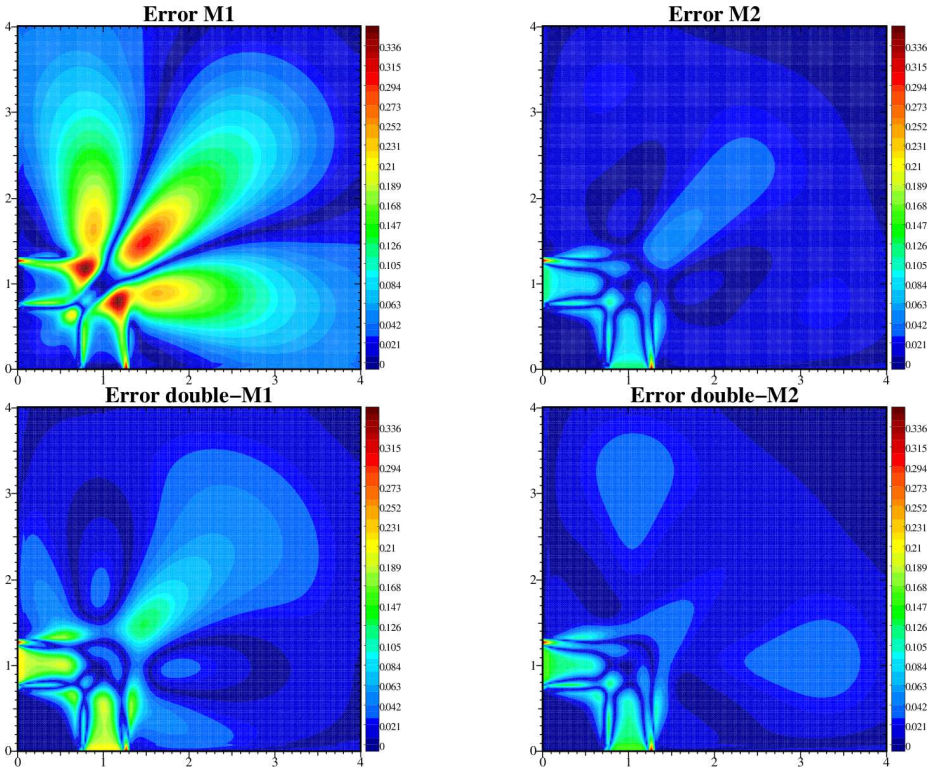

Fig. 15 Absolute error between the doses obtained with Monte-Carlo solver and the M_1 (top left), M_2 (top right), double-M_1 (below left) and double-M_2 solvers (below right) using the approximated closures.

energy were used. The beam is modeled by (33) with the following parameters:

$$\text{at} \quad x = 21.875\ cm, \quad \text{with} \quad y \in [18\ cm, 20\ cm]:$$
$$\varepsilon_0 = 10\ MeV, \quad \Omega_p = -e_1, \quad c_e = 200 \qquad \text{and} \quad c_o = 10^3.$$

The isodose curves at 5%, 10%, 25%, 50%, 70% and 80% of the maximum dose obtained with the different models are plotted on Fig. 16, and the computational times are given in Table 7. As in the previous test cases, the dose computed with the M_1 solver is more diffusive

Model	Monte-Carlo	approximated M_1	approximated M_2
Computation times	$\approx$ 14 h	242 sec $\approx$ 4 min	906 sec $\approx$ 15 min

Table 7 Characteristics of the computations with the different models

than the others. In particular, the dose in the lungs (the dark regions) is overestimated. With both moment models, the dose is underestimated at the entry in the region corresponding to the backbone.

To characterize the errors when considering heterogeneous media, the 3% - 3 mm distance-to-agreement is often used. A voxel is within this agreement if the absolute error in the dose

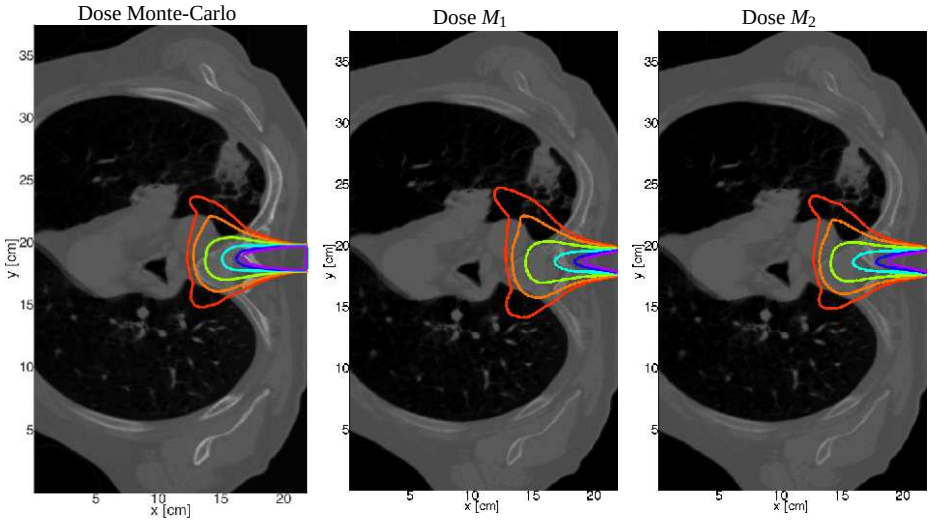

Fig. 16 Dose produced by a 10 MeV electron beam in a cut of a chest using PENELOPE Monte-Carlo solver (left), a M_1 solver (middle) and a M_2 solver (right), with the approximated closures.

compared to the reference at this point is lower than 3% of the maximum dose or if the dose obtained with the reference code at this point is also obtained with the moment code in a radius of less than 3mm around this voxel.

The percentage of voxels not satisfying the 3% - 3 mm distance-to-agreement with the approximated M_1 and M_2 model compared to the reference Monte-Carlo solver for this test case are gathered in Table 8. For both models these voxels are located at the entry on both sides of the beam. For the M_1 model such voxels are also found in the middle of the medium between 4 and 5 cm depth (in the backbone).

Model	approximated M_1	approximated M_2
Percentage of voxels	0.12%	0.054%

Table 8 Percentage of voxels not satisfying the 3% - 3 mm distance-to-agreement compared to the reference Monte-Carlo dose for the 2D simple beam test case in a chest.

See also [45] for more applications of those models in photon transport for radiotherapy.

5 Conclusion

We have proposed an approximation of the M_2 closure and have shown this model to be significantly better than the M_1 model. This approximation is based on the construction of entropy-based closures and the hierarchical structure of such models. In particular, the approximate closure is consistent with the exact closure for the moments associated with isotropic, M_1, 1D, or 2D distributions. Numerical tests show that the M_2 model is much more accurate than the M_1 model and is valid for a larger range of physical phenomena. The

dose computed from the M_2 model is close to the one provided by a reference Monte-Carlo code and required a much lower computational time (between fifty and two hundred times faster).

Future work includes a comparison against optimization methods [27,2,1] which were specifically designed for entropy closures. Furthermore, we plan to generalize our physical model to the coupled system of photons, electrons and positrons, and include bremsstrahlung as well as pair production. We expect that these refinements make the dose calculation accurate enough for clinical purposes.

A Computation of moments in H^i

A.1 Computation of moments in H^1

Consider $\bar{\lambda} \in \mathscr{L}_1$, and the associated ansatz ψ_1 (defined in (21a)) and its moments (ψ^1, ψ^2) given by

$$\begin{aligned} \psi_1(\Omega) &= \exp\left(\lambda_1\Omega_1 + \lambda_4\Omega_1^2 + \lambda_5\Omega_2^2 + \lambda_6\Omega_3^2\right), \\ (\psi^1, \psi^2) &= \langle (\Omega,\ \Omega\otimes\Omega)\psi_1 \rangle \in H^1. \end{aligned}$$

One can remark that ψ_1 is an even function of Ω_2 or Ω_3, and therefore the moment of ψ_1 according to any odd polynomial is zero, in particular

$$\psi_2^1 = \psi_3^1 = \psi_{1,2}^2 = \psi_{1,3}^2 = \psi_{2,3}^2 = 0.$$

With those computations, the moments ψ^1 and ψ^2 actually reads

$$\psi^1 = \psi_1^1 e_1, \quad \psi^2 = Diag\left(\psi_{1,1}^2, \psi_{2,2}^2, \psi_{3,3}^2\right),$$

and ψ^1 is therefore an eigenvector of ψ^2. Using Notations 1 leads to write N^1 and N^2 under the form (23a), and one may obsereve that the eigenvectors of $N^2 - N^1 \otimes N^1$ are along the cartesian axis e_i.

Using again evenness of ψ_1, one obtains

$$\psi_{1,1,2}^2 = \psi_{1,1,3}^2 = \psi_{1,2,3}^2 = \psi_{2,2,2}^2 = \psi_{2,2,3}^2 = \psi_{2,2,3}^2 = \psi_{3,3,3}^2 = 0.$$

Using the fact that $tr(\Omega\otimes\Omega) = 1$, one obtains that

$$\sum_{j=1}^{3} \psi_{i,j,j}^3 = \int_{S^2} \Omega_i tr(\Omega\otimes\Omega)\psi_1(\Omega)d\Omega = \psi_i^1.$$

This leads to write N^3 under the form (24a).

Proposition 4 *Consider realizable moments $(\psi^0, \psi^1, \psi^2) \in \mathscr{R}_2$ such that ψ^1 is an eigenvector of ψ^2.*
Then the rotated normalized moments (N^1, N^2) given by (17) *are in H^1.*

Proof Under those hypothesis, the decomposition (17) can be simplified. Indeed, since ψ^1 is an eigenvector of ψ^2, then N^1 is an eigenvector of N^2. So a rotation R diagonalizing N^2 will send N^1 onto one of the cartesian axis (chose R such that N^1 is along e_1).

Then this rotation also diagonalizes $N^2 - N^1 \otimes N^1$ since it diagonalizes both N^2 and $N^1 \otimes N^1$ and one can write N^1 and N^2 under the form (21a).

Finally one can prove that the unique exponential representation for moments (N^1, N^2) satisfying (23a) is (21a) by using Theorem 1 with $\bar{m}(\Omega) = (\Omega_1,\ \Omega_1^2,\ \Omega_2^2,\ \Omega_3^2)$. Indeed this theorem provide the existence of a unique function ψ of the form (21a) satisfying

$$(N_1^1, N_{1,1}^2, N_{2,2}^2, N_{3,3}^2) = \langle \bar{m}\psi \rangle .$$

Computing the other moments of such a function (21a) read

$$\psi_2^1 = \psi_3^1 = \psi_{1,2}^2 = \psi_{1,3}^2 = \psi_{2,3}^2 = 0,$$

i.e. it satisfies the other moment constraints. Then the unique function (10) satisfying all the moment constraints has the form (21a).

A.2 Computation of moments in H^2

Consider $\bar{\lambda} \in \mathscr{L}_2$, and the associated ansatz ψ_2 (defined in (21b)) and its moments (ψ^1, ψ^2) given by

$$\begin{aligned} \psi_2(\Omega) &= \exp\left(\lambda_5 + \lambda_1\Omega_1 + (\lambda_4 - \lambda_5)\Omega_1^2\right), \\ (\psi^1, \psi^2) &= \langle (\Omega,\ \Omega\otimes\Omega)\psi_2 \rangle \in H^2. \end{aligned}$$

The computations of the previous subsection hold. Since ψ_2 does not depend on Ω_2 nor Ω_3, one deduces that

$$\begin{aligned} \psi^2_{2,2} &= \int_{S^2} \Omega_2^2 \exp\left(\lambda_5 + \lambda_1\Omega_1 + (\lambda_4 - \lambda_5)\Omega_1^2\right) d\Omega = \frac{\psi^0}{2}, \\ \psi^2_{3,3} &= \int_{S^2} \Omega_3^2 \exp\left(\lambda_5 + \lambda_1\Omega_1 + (\lambda_4 - \lambda_5)\Omega_1^2\right) d\Omega = \frac{\psi^0}{2}, \end{aligned}$$

in particular, $\psi^2_{2,2} = \psi^2_{3,3}$. Using Notations 1 leads to write N^1 and N^2 under the form (23b).

Similarily, one has

$$\begin{aligned} \psi^2_{1,2,2} &= \int_{S^2} \Omega_1\Omega_2^2 \exp\left(\lambda_4 + \lambda_1\Omega_1\right) d\Omega = \frac{\psi^1_1}{2}, \\ \psi^2_{1,3,3} &= \int_{S^2} \Omega_1\Omega_3^2 \exp\left(\lambda_4 + \lambda_1\Omega_1\right) d\Omega = \frac{\psi^1_1}{2}, \end{aligned}$$

This leads to write N^3 under the form (24b).

Proposition 5 *Consider realizable moments $(\psi^0, \psi^1, \psi^2) \in \mathscr{R}_2$ such that ψ^1 is an eigenvector of ψ^2 and $\psi^2_{2,2} = \psi^2_{3,3}$.*

Then the rotated normalized moments (N^1, N^2) given by (17) *are in H^2.*

The proof is identical to the one of Proposition 4 with $\bar{m}(\Omega) = (1, \Omega_1, \Omega_1^2)$.

A.3 Computation of moments in H^3

Consider $\bar{\lambda} \in \mathscr{L}_3$, and the associated ansatz ψ_3 (defined in (21c)) and its moments (ψ^1, ψ^2) given by

$$\begin{aligned} \psi_3(\Omega) &= \exp\left(\lambda_4 + \lambda_1\Omega_1\right), \\ (\psi^1, \psi^2) &= \langle (\Omega,\ \Omega\otimes\Omega)\psi_3 \rangle \in H^2. \end{aligned}$$

The computations of the previous subsections hold. In this case, the ansatz ψ_3 is the M_1 ansatz defined in (13), and therefore $\psi^2_{1,1}$ is the Eddington factor χ_2 defined in Subsection 2.3. Using Notations 1 leads to write N^1 and N^2 under the form (23c).

The form of N^3 is not simplified compared to the previous case.

Proposition 6 *Consider realizable moments $(\psi^0, \psi^1, \psi^2) \in \mathscr{R}_2$ such that ψ^1 is an eigenvector of ψ^2, $\psi^2_{2,2} = \psi^2_{3,3}$ and $\psi^2_{1,1} = \psi^0\chi_2\left(|\psi^1|/\psi^0\right)$.*

Then the rotated normalized moments (N^1, N^2) given by (17) *are in H^2.*

The proof is identical to the one of Proposition 4 with $\bar{m}(\Omega) = (1,\ \Omega_1)$.

Acknowledgements The authors are grateful to Gabriele Birindelli (Université de Bordeaux) and Kerstin Küpper (RWTH Aachen) for performing the PENELOPE simulations, and to Nuria Escobar Corral (Uniklinikum RWTH Aachen) for providing the density map in the chest for the last test case.
T. Pichard's PhD was funded by IdEx Bordeaux and Aquitaine Region. This work was also partially funded by Aquitaine Region and FEDER fund through IOPRA interface.

References

1. G. W. Alldredge, C. D. Hauck, D. P. O'Leary, and A. L. Tits. Adaptive change of basis in entropy-based moment closures for linear kinetic equations. *J. Comput. Phys.*, 74(4), february 2014.
2. G. W. Alldredge, C. D. Hauck, and A. L. Tits. High-order entropy-based closures for linear transport in slab geometry II: A comutational study of the optimization problem. *SIAM J. Sci. Comput.*, 34(4):361–391, 2012.
3. G. W. Alldredge, R. Li, and W. Li. Approximating the M_2 method by the extended quadrature method of moments for radiative transfer in slab geometry. *Kin. rel. Mod.*, To appear:–, 2016.
4. A. M. Anile and S. Pennisi. Thermodynamic derivation of the hydrodynamical model for charge transport in semiconductors. *Phys. Rev. B*, 46:13186–13193, 1992.
5. J. Berntsen, T. O. Espelid, and A. Genz. Algorithm 698: Dcuhre: An adaptive multidemensional integration routine for a vector of integrals. *ACM T. Math. Software*, 17(4):452–456, 1991. `http://netlib.org/toms/`.
6. C. Berthon, P. Charrier, and B. Dubroca. An HLLC scheme to solve the M_1 model of radiative transfer in two space dimensions. *J. Sci. Comput.*, 31(3):347–389, 2007.
7. C. Berthon, M. Frank, C. Sarazin, and R. Turpault. Numerical methods for balance laws with space dependent flux: application to radiotherapy dose calculation. *Commun. Comput. Phys.*, 10(5), 2011.
8. J. Borwein and A. Lewis. Duality relationships for entropy-like minimization problems. *SIAM J. Control Optim.*, 29(2):325–338, 1991.
9. J. Borwein and A. Lewis. Partially finite convex programming, Part I: Quasi relative interiors and duality theory. *Math. Program.*, 57:15–48, 1992.
10. J. Borwein and A. Lewis. Partially finite convex programming: Part II. *Math. Program.*, 57:49–83, 1992.
11. T. A. Brunner and J. P. Holloway. One-dimensional riemann solvers and the maximum entropy closure. *J. Quant. Spectros. Radiat. Transfer*, 69(5):543 – 566, 2001.
12. J. Caron, J.-L. Feugeas, B. Dubroca, G. Kantor, C. Dejean, G. Birindelli, T. Pichard, Ph. Nicolaï, E. d'Humières, M. Frank, and V. Tikhonchuk. Deterministic model for the transport of energetic particles. application in the electron radiotherapy. *Phys. Medica*, 31:912–921, 2015.
13. S. Chandrasekhar. *Radiative transfer*. Dover, 1950.
14. I. J. Chetty, B. Curran, J. E. Cygler, J. J. DeMarco, G. Ezzell, B. A. Faddegon, I. Kawrakow, P. J. Keall, H. Liu, C.-M. C. Ma, D. W. O. Rogers, J. Seuntjens, D. Sheikh-Bagheri, and J. V. Siebers. Report of the AAPM task group no. 105: Issues associated with clinical implementation of Monte Carlo-based photon and electron external beam treatment planning. *Medical Physics*, 34(12):4818–4853, 2007.
15. R. Curto and L. A. Fialkow. Recusiveness, positivity, and truncated moment problems. *Houston J. Math.*, 17(4):603–634, 1991.
16. R. Curto and L. A. Fialkow. A duality prood to Tchakaloff's theorem. *J. Math. Anal. Appl.*, 269:519–536, 2002.
17. B. Dubroca and J.L. Feugeas. Hiérarchie des modèles aux moments pour le transfert radiatif. *C. R. Acad. Sci. Paris*, 329:915–920, 1999.
18. B. Dubroca and M. Frank. An iterative method for transport equations in radiotherapy. *Progress in Industrial Mathematics at ECMI 2008*, pages 407–412, 2010.
19. R. Duclous, B. Dubroca, and M. Frank. A deterministic partial differential equation model for dose calculation in electron radiotherapy. *Phys. Med. Biol.*, 55:3843–3857, 2010.
20. J. Sempau F. Salvat, J. M. Fernández-Varea. *PENELOPE-2011: A Code System for Monte Carlo Simulation of Electron and Photon Transport*, 2011.
21. K. O. Friedriechs and P. D. Lax. Systems of conservation equations with a convex extension. *Proc. Nat. Acad. Sci. USA*, 68(8):1686–1688, 1971.
22. H. Grad. On the kinetic theory of rarefied gases. *Commun. Pur. Appl. Math.*, 2(4):331–407, 1949.
23. S. Guisset, S. Brull, B. Dubroca, E. d'Humières, S. Karpov, and I. Potapenko. Asymptotic-preserving scheme for the Fokker-Planck-Landau-Maxwell system in the quasi-neutral regime. *to appear in Commun. Comput. Phys.*, 2015.
24. S. Guisset, J.G. Moreau, R. Nuter, S. Brull, E. d'Humieres, B. Dubroca, and V.T. Tikhonchuk. Limits of the M_1 and M_2 angular moments models for kinetic plasma physics studies. *J. Phys. A: Math. Theo.*, 48(33), 2015.
25. A. Harten, P. Lax, and B. Van Leer. On upstream differencing and Gudonov-type schemes for hyperbolic conservation laws. *SIAM Rev.*, 25(1):35–61, 1983.
26. C. Hauck and R. McClarren. Positive P_N closures. *SIAM J. Sci. Comput.*, 32(5):2603–2626, 2010.
27. C. D. Hauck. High-order entropy-based closures for linear transport in slab geometry. *Commun. Math. Sci*, 9(1):187–205, 2011.
28. C. D. Hauck, C. D. Levermore, and A. L. Tits. Convex duality and entropy-based moment closures: Characterizing degenerate densities. *SIAM J. Control Optim.*, 2007.

29. H. Hensel, R. Iza-Teran, and N. Siedow. Deterministic model for dose calculation in photon radiotherapy. *Phys. Med. Biol.*, 51:675–693, 2006.
30. M. Junk. Maximum entropy for reduced moment problems. *Math. Mod. Meth. Appl. S.*, 10(1001–1028):2000, 1998.
31. D. Kershaw. Flux limiting nature's own way. Technical report, Lawrence Livermore Laboratory, 1976.
32. E. W. Larsen, M. M. Miften, B. A. Fraass, and I. A. Bruinvis. Electron dose calculations using the method of moments. *Med. Phys.*, 24(1):111–125, 1997.
33. C. D. Levermore. Relating Eddington factors to flux limiters. *J. Quant. Spectros. Radiat. Transfer*, 31:149–160, 1984.
34. C. D. Levermore. Moment closure hierarchies for kinetic theories. *J. Stat. Phys.*, 83(5–6):1021–1065, 1996.
35. E. E. Lewis and W. F. Miller. *Computational methods of neutron transport*. American nuclear society, 1993.
36. J. Mallet, S. Brull, and B. Dubroca. An entropic scheme for an angular moment model for the classical Fokker-Planck-Landau equation of electrons. *Commun. Comput. Phys.*, 15(2):422–450, 2014.
37. J. Mallet, S. Brull, and B. Dubroca. General moment system for plasma physics based on minimum entropy principle. *Kin. rel. mod.*, 8(3):533–558, 2015.
38. Maple^{TM}. Technical report, Maplesoft, a division of Waterloo Maple Inc., 2016.
39. P. Mayles, A. Nahum, and J.C. Rosenwald, editors. *Handbook of radiotherapy physics: Theory and practice*. Taylor & Francis, 2007.
40. R. G. McClarren and C. D. Hauck. Robust and accurate filtered spherical harmonics expansion for radiative transfer. *J. Comput. Phys.*, pages 5597–5614, october 2010.
41. J. McDonald and M. Torrilhon. Affordable robust moment closures for cfd based on the maximum-entropy hierarchy. *J. Comput. Phys.*, 251:500–523, 2013.
42. L. R. Mead and N. Papanicolaou. Maximum entropy in the problem of moments. *J. Math. Phys.*, 25(8):2404–2417, 1984.
43. J. J. Moré, B. S. Garbow, and K. E. Hillstrom. *User Guide for MINPACK-1*, 1980. `http://www.netlib.org/minpack/`.
44. E. Olbrant and M. Frank. Generalized Fokker-Planck theory for electron and photon transport in biological tissues: application to radiotherapy. *Comput. Math. Methods Med.*, 11(4):313–339, 2010.
45. T. Pichard, G.W. Alldredge, S. Brull, B. Dubroca, and M. Frank. The M_2 model for dose simulation in radiation therapy. *Proc. Int. Conf. Transport Theory*, 2015.
46. T. Pichard, D. Aregba-Driollet, S. Brull, B. Dubroca, and M. Frank. Relaxation schemes for the M_1 model with space-dependent flux: application to radiotherapy dose calculation. *to appear in Commun. Comput. Phys.*, 2014.
47. R. Piessens, E. De Doncker-Kapenga, and C. W. Überhuber. *QUADPACK: a subroutine package for automatic integration*, springer edition, 1983. `http://www.netlib.org/quadpack/`.
48. G. C. Pomraning. The Fokker-Planck operator as an asymptotic limit. *Math. Mod. Meth. Appl. S.*, 2(1):21–36, 1991.
49. S. La Rosa, G. Mascali, and V. Romano. Exact maximum entropy closure of the hydrodynamical model for Si semiconductors: The 8-moment case. *SIAM J. Appl. Math.*, 70(3):710–734, 2009.
50. F. Schneider. Kershaw closures for linear transport equations in slab geometry I: Model derivation. *J. Comput. Phys.*, pages –, 2016.
51. J. Schneider. Entropic approximation in kinetic theory. *ESAIM-Math. Model. Num.*, 38(3):541–561, 2004.
52. E. Spezi and G. Lewis. An overview of Monte Carlo treatment planning for radiotherapy. *Radiat. Prot. Dos.*, 131(1):123–129, 2008.
53. V. Vikas, C. D. Hauck, Z. J. Wang, and R.O. Fox. Radiation transport modeling using extended quadrature method of moments. *J. Comput. Phys.*, 246:221 – 241, 2013.
54. T.A. Wareing, J.M. McGhee, Y. Archambault, and S. Thompson. Acuros XB ® advanced dose calculation for the Eclipse ^{TM} treatement planning system. *Clinical perspectives*, 2010.
55. C. Zankowski, M. Laitinen, and H. Neuenschwander. Fast electron monte carlo for eclipse^{TM}. Technical report, Varian Medical System.